A chromatinized origin reduces the mobility of ORC and MCM through interactions and spatial constraint

Humberto Sánchez[1], Zhaowei Liu[1], Edo van Veen[1], Theo van Laar[1], John F. X. Diffley[2], and Nynke H. Dekker[1*]

Affiliations:

[1]Department of Bionanoscience, Kavli Institute of Nanoscience, Delft University of Technology, Delft, The Netherlands.
[2] Chromosome Replication Laboratory, Francis Crick Institute, London, UK.

*Correspondence: n.h.dekker@tudelft.nl

ABSTRACT

Chromatin replication involves the assembly and activity of the replisome within the nucleosomal landscape. At the core of the replisome is the Mcm2-7 complex (MCM), which is loaded onto DNA after binding to the Origin Recognition Complex (ORC). In yeast, ORC is a dynamic protein that diffuses rapidly along DNA, unless halted by origin recognition sequences. However, less is known about the dynamics of ORC proteins in the presence of nucleosomes and attendant consequences for MCM loading. To address this, we harnessed an *in vitro* single-molecule approach to interrogate a chromatinized origin of replication. We find that ORC binds the origin of replication with similar efficiency independently of whether the origin is chromatinized, despite ORC mobility being reduced by the presence of nucleosomes. Recruitment of MCM also proceeds efficiently on a chromatinized origin, but subsequent movement of MCM away from the origin is severely constrained. These findings suggest that chromatinized origins in yeast are essential for the local retention of MCM, which may facilitate subsequent assembly of the replisome.

KEYWORDS

DNA replication, yeast replication, replication origin, chromatin, nucleosomes, ORC, Mcm2-7/Cdt1, MCM, target search, protein diffusion

34 **INTRODUCTION**

35 Eukaryotic genomes are structurally organized as a combination of DNA and proteins known
36 as chromatin. Cell biology, genetics, and biochemical experiments have demonstrated that
37 the quantity and local density of the basic structural unit of chromatin, the nucleosome, can
38 define where the initiation of DNA replication happens and that chromatin folding influences
39 replication timing[1]. Less is known about the influence of nucleosomes on the individual
40 proteins that are involved in establishing DNA replication, including their attendant dynamics.
41

42 DNA replication in eukaryotes occurs during the S phase of the cell cycle, during which the
43 entire genome must be duplicated in a coordinated manner. In the budding yeast
44 *Saccharomyces cerevisiae*, replication is initiated from hundreds of sequence-specific origins
45 of replication. Each origin is prepared for replication initiation in two temporally separated
46 steps that are essential for proper DNA replication[2]. During the G1 phase of the cell cycle, the
47 Origin Recognition Complex (ORC) first binds to replication origins[3]. These origins are
48 autonomous replicating sequences (ARS) that contain both a strong binding site (the ARS
49 consensus sequence, or ACS) and a weak binding site (B2) for ORC. Once bound, ORC, together
50 with Cdc6 and Cdt1, then loads two inactive Mcm2-7 (MCM) replicative DNA helicases,
51 forming the pre-replication complex (pre-RC); this is known as the licensing step[4, 5]. During S
52 phase, origins of replication are activated by the combined action of two kinases, S-CDK and
53 DDK, and several other proteins known as firing factors, which serve to bring Cdc45 and GINS
54 into association with MCM and form the CMG holo-helicase[6-8]. The addition of DNA
55 polymerases as well as accessory proteins completes the assembly of the full replisome and
56 allows DNA replication to proceed[8, 9].
57

58 During the licensing step, ORC, Cdc6 and MCM/Cdt1 load at DNA replication origins that are
59 embedded in the chromatin[2]. Biochemical studies have shown that such origins are free of
60 nucleosomes[10], and genome-wide analysis suggests that these specific nucleosome-free
61 regions (NFRs) favor ORC binding[11]. Interestingly, ORC then plays an active role in positioning
62 nucleosomes around the origin[11, 12] by coordinating the activity of chromatin remodelers
63 before and during replication[12, 13]. Chromatin remodelers that act at the origin also influence
64 origin licensing[14].
65
66 We have previously demonstrated that yeast ORC is a mobile protein that rapidly diffuses on
67 bare DNA, but that origin recognition halts this search process[15]. Furthermore, it has been
68 observed that single and double MCM hexamers diffuse on DNA[4, 5] and that nucleosomes can
69 act as potential obstacles for MCM diffusion[16], so we sought to investigate the roles of origin-
70 flanking nucleosomes in either directly limiting or locally targeting the diffusion of ORC and,
71 consequently, in the loading of MCM onto DNA.
72
73 **RESULTS**
74 **Establishment of a labeled chromatinized origin of replication within 10.4 kbp DNA for**
75 **single-molecule investigations**
76 To experimentally examine the origin localization and dynamics of ORC and MCM on a
77 chromatinized origin of replication, we designed an *in vitro* single-molecule force-
78 fluorescence assay using purified yeast proteins (**Supplementary Figure 1.1**). We wished to
79 visualize the chromatinized origin using yeast histone octamers marked with fluorescent
80 labels. To achieve this, we first introduced a single cysteine on the H2A histone by replacing
81 residue lysine 120 (K120), which avoids disruption of the overall nucleosome structure (**Figure**

82 **1a**; Methods). Purified yeast histone octamers containing two H2A (K120C) histones were
83 then covalently bound with one single AF488 dye per cysteine (degree of labeling p_{label} = 0.81,
84 as determined from bulk experiments; Methods). We next engineered an ARS1 origin of
85 replication flanked by two nucleosome positioning sequence (NPS) sites spaced by 150 bp (50
86 nm) (Ref. 16 and Methods), and reconstituted fluorescently labeled nucleosomes onto these
87 NPS sites using salt gradient dialysis. The resulting chromatinized origin tested positively for
88 *Pst*I restriction digestion between the nucleosomes (**Supplementary Figure 1.2b**), which
89 indicated that it should remain accessible to ORC and MCM. Next, we ligated this
90 chromatinized origin to two biotinylated DNA fragments of distinct sizes. This resulted in a
91 10.4 kbp chromatinized DNA molecule (**Figure 1b**) in which the origin was localized at
92 approximately one third of the total length of the DNA molecule (**Supplementary Figure 1.2c**).
93 In addition to the ARS1 origin, the 10.4 kbp DNA molecule contained a number of endogenous
94 potential binding sites for ORC[17] and regions of high AT content (**Supplementary Figure 1.2d**).
95
96 Following preparation, the 10.4 kbp DNA molecules including a chromatinized origin were
97 introduced into the microfluidic flow cell of our single-molecule instrument. Here, the DNA
98 molecules were tethered to streptavidin-coated beads in a dual-beam optical trap, after
99 which they were visualized in a protein-free channel of the flow cell (buffer channel) while
100 under a tension of 2 pN. Nucleosome-bound AF488-H2A was detected as a bright fluorescent
101 spot (or focus) whose spatial position was determined (**Figure 1b**). By repeating this
102 measurement on multiple DNA molecules, we could build up the spatial distribution of H2A
103 foci as a function of genomic coordinate. As each individual DNA molecule was tethered in
104 one of two possible orientations in the dual-beam optical trap, we report spatial distributions
105 from the midpoint of the DNA. Each histogram bin (width 0.670 kbp; Methods) thus contains

106 the average of the occupancies of two segments of DNA located symmetrically about the
107 midpoint of the DNA: for example, the origin bin contains the mean of the occupancies of the
108 actual origin- and NPS-containing segment and the DNA segment located oppositely from the
109 midpoint of the DNA by 1.7 kbp. The spatial distribution of H2A fluorescent foci (filtered to
110 remove foci containing more than 4 H2A, which could represent aggregates; Methods)
111 showed a clear peak in the bin containing the NPS sites (left panel in **Figure 1c**), suggesting
112 preferential nucleosome assembly at the NPS sites. This spatial distribution of H2A was built
113 up from distinct DNA samples chromatinized on different days, which exhibited only minimal
114 differences between them (**Supplementary Figure 1.4**), highlighting the reproducibility of our
115 sample preparation.
116
117 Ideally, our chromatinized origin should contain two fluorescently labeled nucleosomes
118 within a single diffraction-limited spot. Assuming that the identification of a single
119 fluorescently labeled H2A reflects the presence of a single H2A-H2B dimer bound to a H3-H4
120 tetramer, we should then measure 4 fluorescently labeled H2A per focus. However, the
121 experimental counts of fluorescently labeled H2A may be reduced by non-unity values for the
122 probability of occupancy of the two NPSs ($p_{occupancy}$), the probability of H2A-H2B dimer
123 association to the H3-H4 tetramer (p_{h2a}), and p_{label} (**Supplementary Figure 1.3a**). To count the
124 number of labeled H2A, we identified step-wise photobleaching events using Change-Point
125 Analysis (CPA; Methods), whereby the methodology is assessed and validated using dCas9
126 tagged and labeled identically to H2A (**Supplementary Figure 1.1**). The lifetime prior to
127 photobleaching of AF488 when linked to H2A was similar to that measured when it was linked
128 to dCas9, indicating that labeled H2A are stable on the DNA during the experiment
129 (**Supplementary Figure 1.3c**). Using this photobleaching approach, we found that the H2A

130 foci primarily contained two to three AF488-labeled H2A histones, as shown in the
131 stoichiometry distribution (right panel in **Figure 1c**) built up from a total of N_{DNA} = 247 derived
132 from the four different chromatinized DNA samples mentioned above (again exhibiting only
133 minimal differences between them, **Supplementary Figure 1.4**). With the independently
134 measured p_{label} = 0.81 as fixed parameter, the best fit to the experimentally determined
135 stoichiometry distribution **(Figure 1c**, with mean squared error (MSE) = 5.18 x 10^{-5} and fit
136 values described by white numbers inside the bar plot; **Supplementary Figure 1.3b**) yielded
137 $p_{occupancy}$ = 1.00 (corresponding to full occupancy of the NPSs) and p_{h2a} = 0.77.
138
139 To confirm that the detected fluorescent H2A foci reflected embedding of H2A into
140 nucleosomes – as opposed to unspecific electrostatic interactions of H2A-H2B dimers with
141 the DNA[18] – we separately probed for nucleosome presence on our 10.4 kbp DNA using force
142 spectroscopy. Previous experiments have shown that under force, DNA can be unwrapped
143 from the histone octamer. Irreversible jumps in the force-extension curve in which 27 nm (80
144 bp) of DNA is unwrapped from either a hexasome or a full nucleosome have been reported
145 to occur over a broad range of forces (8-40 pN) [19-22]. Indeed, when we pulled on one extremity
146 of a tethered chromatinized DNA molecule with labeled H2A histones at a constant speed
147 (100 nm/s) (**Supplementary Figure 1.5a**), we could identify such jumps (**Supplementary**
148 **Figure 1.5b**). These occurred at a force of 17.6 pN ± 5.8 pN (mean ± standard deviation) and
149 yielded contour length increments of 24.8 nm ± 5.9 nm (mean ± standard deviation), the latter
150 corresponding to the contour length of the unwrapped DNA. At least two such jumps were
151 revealed in 88.5% of the chromatinized DNA molecules probed (**Supplementary Figure 1.5c**),
152 implying that our chromatinized DNA typically contains two nucleosomes (or hexasomes).
153

154 Together, these single-molecule fluorescence and force spectroscopy results support our
155 establishment of a 10.4 kbp DNA containing a single origin of replication flanked by two
156 nucleosomes. As the force spectroscopy does not report on nucleosome location, however,
157 to investigate the influence of a chromatinized origin of replication on ORC and MCM, we
158 focused on fluorescence readouts alone.
159
160 **Nucleosomes enhance intrinsic ORC preference for the origin of replication**
161 To study the effect of chromatinized origins on ORC binding and dynamics, we labeled the N-
162 terminus of the Orc3 subunit with a JF646 fluorophore via a HaloTag (Methods). We
163 confirmed that the labeled ORC could load MCM in bulk assays (**Supplementary Figure 1b**).
164 We then prepared four different 10.4 kbp DNA molecules that either contained ARS1 or a
165 mutated origin without specific affinity for ORC[15, 23], and that were chromatinized or not.
166
167 We first performed experiments that report on the rapid binding of ORC to a chromatinized
168 origin. To do so, we incubated the optically trapped DNA molecule held at near-zero force in
169 a reservoir of the microfluidic flowcell containing 5 nM JF646-ORC for 5 s. Subsequently, we
170 shifted the DNA to a separate, protein-free channel and imaged it under a stretching force of
171 2 pN (**Figure 2a**). DNA-bound JF646-ORC could then be observed as a bright fluorescent spot
172 (focus), after which the experiment was repeated with a new DNA. Stoichiometric analysis of
173 the foci via step-wise photobleaching indicated that they predominantly contained individual
174 ORC molecules (**Supplementary Figure 2**). Foci containing more than 5 ORCs, which could
175 represent aggregates (Methods), were not analyzed further. The remaining fluorescent foci
176 were observed throughout the DNA molecule, but the overall spatial distribution exhibited
177 clear overrepresentation of ORC in the bin containing the ARS1 origin (30% of the total, **Figure**

178 **2b-i**). This preference for ORC binding in the bin containing the origin[15] increased to 39% when
179 the origin was chromatinized (**Figure 2b-ii**). Mutation of the origin reduced preferential
180 binding by ORC in the bin containing the origin[15]; instead, ORC was observed to peak in an
181 adjacent bin (**Figure 2b-iii**) that included a potential ORC binding site (located at 2.4 kbp from
182 the start of the construct, **Supplementary Figure 1.2d**). Chromatinization of this mutated
183 origin nonetheless increased ORC presence in the origin bin from 14% to 26% (**Figure 2b-iii,**
184 **2b-iv**). For the four conditions probed, ORC binding in the bin containing the origin
185 (chromatinized or not) was subjected to tests of statistical significance (**Figure 2c**). These
186 results indicate a statistically significant enhancement of ORC binding in the presence of
187 either ARS1 or nucleosomes, with the effect of the former being more pronounced.
188
189 **Nucleosomes flanking the origin reduce ORC mobility and increase ORC lifetime**
190 We have previously shown that ORC is a mobile protein that slides on bare DNA[15]. Here we
191 sought to investigate the motion dynamics of ORC on DNA containing a chromatinized origin
192 following rapid binding under the incubation conditions described above (**Figure 2a**). When
193 we tracked the position of ORC molecules initially located in the bin containing the
194 chromatinized origin over time (**Figure 3a-i**, showing 30% of all traces, selected at random), it
195 appeared that within experimental error many of these ORC molecules hardly changed their
196 position. Conversely, ORC molecules initially located outside the origin (**Figure 3a-ii**, showing
197 30% of all traces, selected at random) were observed to explore their local DNA environment
198 in seemingly random fashion, which in some cases allowed them to approach, and then move
199 away from, the nucleosomes.
200

201 To quantify these motion dynamics of ORC, we calculated the mean squared displacement
202 for each ORC molecule on the four types of DNA molecules described above versus time
203 interval and extracted a diffusion constant from a linear fit. Distributions (in log scale) of the
204 fitted diffusion constants are shown in **Figure 3b**. We observed a wide spread of diffusion
205 constants, ranging from 10^{-6} to 10^{0} kbp^2 s^{-1}. Using the Bayesian Information Criterion, we
206 identified kinetically distinct population states for ORC on non-chromatinized DNA containing
207 ARS1 (**Figure 3b-i**). These describe either a population with a low mean diffusion constant
208 (hereafter 'slow ORC population') (D_{slow} = 0.0049 ± 0.0028 kbp^2 s^{-1} (mean ± SEM)) or a
209 population with a higher mean diffusion constant (hereafter 'fast ORC population') (D_{fast} =
210 0.152 ± 0.023 kbp^2 s^{-1}), consistent with our earlier findings for ORC on longer DNA molecules
211 that contained a synthetic origin of replication[15]. We used these means as imposed values in
212 fitting the distribution of ORC diffusion constants obtained on the other three types of DNA
213 molecules (**Figure 3b-ii, 3b-iii,** and **3b-iv**). As one can observe both by eye and from the fits,
214 chromatinization of the ARS1 origin resulted in an increase in the slow ORC population (**Figure**
215 **3b-ii**). On DNA molecules with the mutated origin, the fast ORC population predominated
216 (**Figure 3b-iii**), again consistent with our previous findings[15] but chromatinization of this
217 mutated origin also resulted in an increase in the slow ORC population (**Figure 3b-iv**). We
218 summarize these results more quantitatively by computing the fraction of the slow ORC
219 population in the total, whereby we used the geometric mean D^* (= $10^{(\mu_{slow} + \mu_{fast})/2}$ =
220 0.0065 kbp^2 s^{-1}, where μ_i are the lognormal population means) as a cutoff (**Figure 3c-i**). This
221 fraction was always observed to be higher upon chromatinization of the origin.
222
223 To assess how chromatinization of the origin resulted in an increase of the slow ORC
224 population, we repeated this analysis separately for ORC molecules initially localized in the

225 origin bin (**Figure 3c-ii**) and for ORC molecules initially localized elsewhere (**Figure 3c-iii**). For
226 ORC molecules initially localized in the origin bin, chromatinization of the origin led to an
227 increase in the slow ORC population, irrespective of whether the origin contained ARS1 or
228 was mutated (**Figure 3c-ii**). This reduction in ORC mobility could have resulted solely from the
229 spatial confinement imposed on ORC by the nucleosomes, or additionally through ORC
230 interactions with the nucleosomes. Interestingly, for ORC molecules initially localized
231 elsewhere, chromatinization of the origin also led to an increase in the slow population of
232 ORC molecules, again irrespective of the origin contained ARS1 or was mutated (**Figure 3c-**
233 **iii**). This reduction in ORC mobility suggested ORC interactions with the nucleosomes.
234
235 To address whether chromatinization of the origin influenced the stability of ORC binding, we
236 examined the lifetimes of individual JF646 dyes on DNA-bound ORC molecules by tracking foci
237 containing 1 or 2 ORC molecules at 0.6 s/frame until the fluorescence signal disappeared.
238 Apart from on the DNA molecule with the chromatinized mutated origin, the mean lifetime
239 of ORC was shorter than 30 s, making it substantially shorter than the bleaching-limited mean
240 lifetime of JF646 measured under identical imaging conditions (71.0 s, **Supplementary Figure**
241 **1.1c**) by attaching it to DNA-bound dCas9. This indicated that ORC molecules typically
242 dissociated from DNA during the measurement, in accord with our previous observations[15].
243 Nonetheless, the mean lifetime of the slow ORC population typically exceeded that of the fast
244 ORC population (**Supplementary Figure 3b**). Of the ORC molecules initially located at or close
245 to the ARS1 origin on bare DNA, 61% were associated with the slow ORC population (red bin,
246 **Figure 3c-ii**); this fraction is increased to 84% upon chromatinization of the ARS1 origin
247 ('bordeaux' bin, **Figure 3c-ii**). While not all of these ORC molecules may be specifically bound
248 to DNA (as also suggested by a corresponding increase in the slow ORC population observed

249 upon chromatinization of the mutated origin, compare grey and pink bins in **Figure 3c-ii**),
250 nonetheless the increase in the slow ORC population with its higher mean lifetime on a
251 chromatinized ARS1 suggests that flanking nucleosomes can contribute to the temporal
252 retention of ORC near an origin of replication. This could in turn contribute to preferential
253 recruitment of MCM there.
254
255 **Stable ORC binding to DNA requires the origin of replication**
256 We also performed experiments with more extended incubation conditions compatible with
257 the timescale required for full maturation of MCM[5, 15]. When performed with ORC and Cdc6
258 only (see next section for experiments involving MCM), these experiments provided a read-
259 out of long-lived, stable ORC binding. Concretely, we incubated ORC and Cdc6 in bulk, for 30
260 min with the four types of DNA molecules (untethered to beads, hence with free ends), prior
261 to imaging in single-molecule conditions. We separately verified that an extended incubation
262 period alone did not affect the distributions of H2A position or stoichiometry on
263 chromatinized DNA (**Supplementary Figure 4.1**). We then introduced these pre-incubated
264 DNA molecules into the flowcell, trapped, them, and imaged stable ORC molecules that
265 remained bound to the DNA (**Figure 4a**).
266
267 Following this experimental approach, on bare DNA molecules containing the ARS1 origin we
268 observed either DNA molecules devoid of ORC ($N_{DNA\text{-}no\ ORC}$ = 10, 21% of total), or DNA
269 molecules ($N_{DNA\text{-}ORC}$ = 38, 79% of total) with ORC. Using the latter, we plotted the spatial
270 distribution of ORC (**Figure 4b-i**). We found that 61% of the ORC foci were localized in the
271 origin bin (N_{foci} = 38, $N_{foci\ in\ origin}$ = 23), which emphasizes the preference of stable ORC binding
272 at the origin compared to the other DNA sequences in the 10.4 kbp DNA[15]. Stoichiometric

273 analysis showed no difference with the experiments reporting on rapid ORC binding (compare
274 **Supplementary Figure 2b-i**, **Supplementary Figure 4.2b-i**). On DNA molecules with a
275 chromatinized ARS1 origin, the overall fraction of DNA molecules containing ORC foci was
276 reduced by a factor of two, to 41% ($N_{DNA\text{-}no\ ORC}$ = 74, $N_{DNA\text{-}ORC}$ = 52). However, we observed a
277 similar fraction (51%) of ORC foci localized in the origin bin (N_{foci} = 43, $N_{foci\ in\ origin}$ = 22, **Figure**
278 **4b-ii**), indicating that chromatinization of ARS1 did not enhance the likelihood of finding ORC
279 stably bound in the origin bin relative to elsewhere on the DNA. Interestingly, stoichiometric
280 analysis showed that such conditions led to an increase in the number of ORC molecules per
281 focus (**Supplementary Figure 4.2b-ii**). When these experiments were repeated on DNA
282 molecules with the mutated origin, we predominantly found DNA molecules devoid of ORC,
283 irrespective of whether nucleosomes were present ($N_{DNA\text{-}no\ ORC}$ = 45, $N_{DNA\text{-}ORC}$ = 2, **Figure 4b-**
284 **iv**) or not ($N_{DNA\text{-}no\ ORC}$ = 32, $N_{DNA\text{-}ORC}$ = 10, **Figure 4b-iii**). This suggested that stable ORC binding
285 probed under these experimental conditions is predominantly associated with DNA
286 sequence. For the four conditions probed, ORC binding in the bin containing the origin
287 (chromatinized or not) was subjected to tests of statistical significance (**Figure 4c**). These
288 results indicate that statistically significant enhancement of stable ORC binding depends on
289 the presence of ARS1, but not on the presence of chromatin.
290
291 Previous studies have shown direct interactions between ORC and nucleosomes, suggesting
292 a potential for nucleosome remodeling by ORC[11, 24]. Thus, we assessed whether in our
293 experiments the presence of ORC and Cdc6 impacted the spatial distribution and
294 stoichiometry of H2A. For reference, following a 30 min buffer-only bulk incubation of the
295 DNA with a chromatinized ARS1 origin (N_{DNA} = 51), 80% of H2A foci were found in the origin
296 bin (N_{foci} = 45, $N_{foci\ in\ origin\ bin}$ = 36), and the best fit of the H2A stoichiometry distribution yielded

297 p_{h2a} = 0.73 and $p_{occupancy}$ = 0.98 (**Supplementary Figure 4.1**), values similar to those obtained
298 without such bulk incubation (**Figure 1c)**. When the bulk incubation was performed in the
299 presence of ORC and Cdc6 (N_{DNA} = 126), however, the fraction of H2A foci in the origin bin
300 was reduced to 49% (N_{foci} = 134, $N_{foci\ in\ origin\ bin}$ = 66) (**Supplementary Figure 4.3b**), and the best
301 fit of the H2A stoichiometry distribution yielded p_{h2a} = 0.81 and $p_{occupancy}$ =0.52. The latter
302 parameters suggested a maintenance of H2A-H2B dimer stability but a less complete NPS
303 occupancy. When the bulk incubation in the presence of ORC and Cdc6 was performed on
304 DNA molecules with a chromatinized mutated origin (N_{DNA} = 47), an intermediate value of
305 64% of H2A foci were found in the origin bin (N_{foci} = 56, $N_{foci\ in\ origin\ bin}$ = 36) (**Supplementary**
306 **Figure 4.3c**), and the best fit of the H2A stoichiometry distributions of H2A yielded p_{h2a} = 0.60
307 and $p_{occupancy}$ = 1.00. The latter parameters indicated a reduction in H2A-H2B dimer stability
308 without a change in NPS site occupancy. In summary, these results show that under these
309 more extended incubation conditions, the presence of ORC and Cdc6 can influence
310 nucleosome positioning and stability.
311
312 **Nucleosomes flanking the origin permit MCM recruitment but restrict subsequent motion**
313 Having probed both rapid and stable ORC binding and established that the presence of ARS1
314 was beneficial to both but the presence of nucleosomes only to the former, we wanted to
315 test how the presence of nucleosomes impacted the loading of MCM. We therefore set out
316 to probe the spatial positioning, stoichiometry, and dynamics of MCM on a chromatinized
317 origin. To visualize MCM, we used JF646-labeled MCM in loading reactions. MCM was labeled
318 by introducing a HaloTag on the N-terminus of its Mcm3 subunit, and JF646-MCM performed
319 normally in a bulk loading assay (**Supplementary Figure 1.1**). We then incubated ORC, Cdc6
320 and MCM/Cdt1 with DNA in bulk, without tethering to beads, for 30 min[5, 15] as described

321 above for the experiments that probed for stable ORC binding. We next introduced these pre-
322 incubated DNA molecules into the flow cell, and imaged JF646-MCM as described above
323 (**Figure 5a**).
324
325 In the absence of nucleosomes, MCM foci were broadly distributed about the ARS1 origin
326 (**Figure 5b-i**), as previously described[15]. Chromatinization of ARS1 origin, however, resulted in
327 a strikingly different situation: MCM foci were now mainly localized in the origin bin (**Figure**
328 **5b-ii**). Repeating this experiment on bare DNA containing the mutated origin again resulted
329 in a broad distribution of MCM (**Figure 5b-iii**), this time with a slight peak in the same bin as
330 was observed in the experiments that probed rapid ORC binding (**Figure 2b-iii**).
331 Chromatinization of this mutated origin did not significantly increase the presence of MCM in
332 the origin bin (**Figure 5b-iv**). For the four types of DNA molecules probed, MCM binding in the
333 bin containing the origin (chromatinized or not) was subjected to tests of statistical
334 significance (**Figure 5c**). These results indicate that chromatinization of the ARS1 origin, but
335 not of a DNA segment without ARS1, statistically significantly increases the population of
336 MCM bound there.
337
338 We also examined the stoichiometry of MCM foci bound to four different types of DNA
339 molecules tested under these four conditions. Stoichiometric analysis showed that the MCM
340 foci predominantly contained 1 or 2 molecules for all cases (**Supplementary Figure. 5.1**).
341 However, foci found on DNA molecules that contained the chromatinized ARS1 origin
342 exhibited the highest fraction of foci in the origin bin that contained 2 MCM molecules (53%,
343 right plot in **Supplementary Figure 5.1-ii**). We discuss this further below, together with the

344 overall observation that the spatial distributions of MCM resembled those obtained for rapid
345 ORC binding (**Figure 2**) more closely than those obtained for stable ORC binding (**Figure 4**).
346
347 As our experiments showed that the presence of ORC and Cdc6 during 30 min incubations in
348 bulk impacted nucleosome positioning and stability (**Supplementary Figure 4.3**), we also
349 monitored nucleosome positioning and stability upon the inclusion of MCM. On DNA
350 molecules with a chromatinized ARS1 (N_{DNA} = 110), 83% of H2A foci were found in the origin
351 bin (N_{foci} = 81, $N_{foci\ in\ origin\ bin}$ = 67), and the best fit of the H2A stoichiometry distribution yielded
352 p_{h2a} = 0.84 and $p_{occupancy}$ = 0.89 (**Supplementary Figure 5.2b**), which are all values similar to
353 those obtained following incubation with buffer alone. However, on DNA with a
354 chromatinized mutated origin (N_{DNA} = 123), only 50% of H2A foci were located in the origin
355 bin (N_{foci} = 70, $N_{foci\ in\ origin\ bin}$ = 140), and the best fit of the H2A stoichiometry distribution
356 yielded p_{h2a} = 0.91 and $p_{occupancy}$ = 0.40. The latter parameters suggested a maintenance of
357 H2A-H2B dimer stability but a less complete NPS site occupancy. We speculate that increased
358 MCM loading on a chromatinized ARS1 origin (**Supplementary Figure 5.2b**) relative to the
359 chromatinized mutated origin (**Supplementary Figure 5.2c**) limits the continued access of
360 ORC and Cdc6 to nucleosomes, and hence their impact (see also Discussion).
361
362 Lastly, we tested whether a pair of nucleosomes surrounding ARS1 can prevent MCM, once
363 loaded, from diffusing outwards away from ARS1. To test this directly, we monitored MCM
364 position over an extensive duration of time by repeated the preceding experiments but
365 imaging JF646-MCM at a 100-fold slower rate (one frame per min, **Figure 5d**). This allowed us
366 to probe for MCM motion occurring on timescales up to approximately 15 min. We measured
367 the relative displacements of JF646-MCM foci every 2 min (or 2 frames) until JF646 was no

368 longer visible due to photobleaching (lifetime of the JF646 dye on DNA-bound dCas9 under
369 identical imaging conditions was 1.23 x 10^3 s). These data were benchmarked relative to the
370 displacement distribution of dCas9 (**Figure 5e-i**) obtained under identical experimental
371 conditions, which was centered about 0 and had a width of σ = 0.061 kbp that derived from
372 experimental noise. The distribution of displacements by MCM on DNA molecules with a bare
373 ARS1 had a substantially increased width relative to dCas9 (**Figure 5f-ii**; σ = 0.398 kbp),
374 indicating one-dimensional diffusion of the MCM foci as previously observed[15]. However, on
375 DNA containing the chromatinized ARS1, the distribution of displacements by MCM again had
376 a narrow width (**Figure 4f-iii**; σ = 0.153 kbp). This indicated that one-dimensional diffusion of
377 MCM away from the ARS1 origin of replication was hampered by the presence of flanking
378 nucleosomes.
379
380 **DISCUSSION**
381 Chromatin replication starts from origins that are flanked by nucleosomes. We have studied
382 at the single-molecule level to understand how the presence of nucleosomes impacts the
383 binding and mobility of ORC in the vicinity of the origin and subsequently, the recruitment
384 and mobility of MCM.
385
386 **Nucleosomes facilitate rapid binding of ORC to the origin and decrease its mobility**
387 Our experiments first probed the rapid binding of yeast ORC to DNA following a short
388 incubation period in the single-molecule instrument (**Figure 2**) and the subsequent motion of
389 these molecules (**Figure 3**). As our previous work on bare DNA has shown, mobile ORC
390 molecules can contribute to origin recognition by scanning the DNA – given the measured
391 diffusion constant of the fast ORC population (**Figure 3b-i**), even during a short 5 s incubation

392 period an individual ORC molecule can scan ~1.2 kbp on bare DNA, which contributes to its
393 observed binding at many different sites along the DNA (**Figure 2b-i**). Repeating these
394 experiments in the presence of a chromatinized origin showed that the presence of
395 nucleosomes provides a mild increase in local ORC binding (**Figure 2b-ii, c**) and a reduction in
396 ORC mobility (**Figure 3b-ii, c**). The latter can derive from spatial confinement of ORC by
397 nucleosomes, direct interactions between ORC and nucleosomes, or a combination thereof.
398 A reduction in ORC mobility can furthermore account for the observed increase in local ORC
399 binding: for example, if nucleosomes similarly reduced the influx of mobile ORC molecules
400 into the origin region and their efflux out of it, then direct interactions between ORC and
401 nucleosomes could account for the observed increase in local ORC binding. Certainly, our data
402 suggest that in the yeast system ORC molecules can readily locate a chromatinized origin via
403 binding from solution even if their one-dimensional diffusion is blocked; whether the same
404 holds true for higher eukaryotes that lack sequence-specific origins remains to be
405 determined.
406
407 **Stable binding of ORC is primarily enabled by the origin of replication**
408 We next asked whether nucleosomes affected the stable binding of ORC to DNA following
409 bulk incubation of ORC with DNA molecules over an extended duration. Examination in the
410 single-molecule instrument revealed that a bare ARS1 origin alone sufficed to retain stably
411 bind ORC molecules to DNA (**Figure 4a**); no further increases in the yield of stable ORC were
412 observed with a chromatinized ARS1 origin (**Figure 4b**). Interestingly, while DNA molecules
413 that contained a mutated origin could recruit rapidly bound ORC (**Figure 2d,e**), they could not
414 stably retain ORC, irrespective of whether nucleosomes surrounded the origin (**Figure 4d,e**).
415 This most likely suggests that rapidly but nonspecifically recruited ORC molecules unbind from

416 the DNA directly into solution[25], as our direct tracking of the motion of ORC does not provide
417 experimental evidence that ORC can bypass flanking nucleosomes (**Figure 3**). These
418 experiments thus showed that ARS1 is required for stable ORC binding[15] even in the presence
419 of nucleosomes. This contrast with results from another study[26] that suggested that a specific
420 sequence might not be necessary and found ORC bound specifically to nucleosomes. Such
421 discrepancies may have resulted from differences in the experimental preparations
422 employed. Nevertheless, our findings are in line with previous findings that show that origin
423 sequences are required for yeast replication *in vitro* on chromatinized DNA and *in vivo* in
424 budding yeast[27, 28].
425
426 Stoichiometric analysis of either rapidly or stably bound ORC molecules bound to the region
427 containing the ARS1 origin indicated an increase in ORC stoichiometry upon chromatinization
428 (**Supplementary Figure 2**). We computed the resulting ratio of 1 ORC molecule:2 ORC
429 molecules to be ~1:3, very similar to the ratio previously determined using cryo-EM[16]. An
430 increase in ORC stoichiometry upon chromatinization of ARS1 could result from a similar
431 influx of ORC to the origin but a reduced efflux as the diffusion of ORC molecules away from
432 the origin[15] is reduced by the presence of nucleosomes, or an increased influx of ORC to the
433 origin due to direct interactions between ORC and nucleosomes[26, 29], or a combination of
434 these effects.
435
436 **Influence of ORC and MCM on nucleosome remodeling at the origin of replication**
437 Previous studies have indicated that ORC has properties of a chromatin remodeler[12-14, 24],
438 either due to direct interaction of ORC with the nucleosomes or due to DNA bending at the
439 origin[30]. Indeed, we confirmed that extended incubation of chromatinized substrates with

440 ORC and Cdc6 could broaden the spatial distribution and/or reduce the stoichiometry of H2A
441 histones embedded within our nucleosomes (**Supplementary Figure 4.3**), in agreement with
442 published work reporting in vitro remodeling of H2A-H2B dimers by ORC[24]. Interestingly, our
443 data monitoring the position and stoichiometry distributions of H2A following an extended
444 incubation with all loading factors, however, show no changes therein on DNA containing a
445 chromatinized ARS1 origin (**Supplementary Figure 5.2**). This suggests a protective role for
446 MCM in the maintenance of epigenetic chromatin states prior to the firing of DNA
447 replication[31].
448
449 **Loading of MCM onto a chromatinized origin**
450 Our results showed that the lack of a replication origin inhibits the stable binding of ORC to
451 DNA (**Figure 4**), but not the rapid binding of ORC (**Figure 2**) or the loading of MCM (**Figure 5**).
452 This implies that stable binding of ORC at ARS1 is not a prerequisite to MCM loading, which is
453 consistent with biochemical experiments showing that MCM loading can occur independently
454 of specific origins[5]. Furthermore, our measurements of the spatial distributions of MCM
455 indicate that for the four types of DNA molecules tested, there is a probability of finding MCM
456 molecules all along the DNA molecule. Several factors underlie this behavior. First, it is the
457 one just mentioned: ORC binding is not strictly sequence-specific even in yeast, and thus MCM
458 loading can occur at different DNA sequences. Indeed, the spatial distribution of MCM
459 molecules (**Figure 5**) showed similar features to the spatial distributions of rapid ORC binding
460 (**Figure 2**)**.** Second, both bulk biochemical assays[4, 5] and our previous single-molecule studies[15]
461 have shown that loaded MCM can undergo linear diffusion on DNA. In the buffer conditions
462 employed, the diffusion constant of MCM equals 0.0008 ± 0.0002 $kbp^2\ s^{-1}$ (**Figure 5e-ii**), from

463 which we estimate that diffusion of MCM during the extended incubation period contributed
464 ~1.4 kbp to the broadening of the observed spatial distribution.
465
466 On DNA molecules containing a chromatinized ARS1, we found that the probability of finding
467 MCM proteins in the vicinity of the origin was increased by more than two-fold compared to
468 that on DNA molecules containing bare ARS1. Given that this increase is larger for MCM
469 (**Figure 5c**) than for rapidly bound ORC (**Figure 2c**), this data alone could suggest that the
470 presence of nucleosomes prevents the diffusion of MCM molecules away from the origin. The
471 lack of a similar increase in the probability of MCM foci close to the origin due to the
472 chromatinization of a mutated origin, compare **Figure 4e** to **Figure 4d** (despite a
473 corresponding mild increase in rapid ORC binding, compare **Figure 2e** to **Figure 2d**) is
474 consistent with previous work showing that nucleosomes reduced non-specific loading of
475 MCM on a mutated origin[14, 32].
476
477 Stoichiometric analysis reveals that the detected MCM foci in region of the ARS1 origin
478 predominantly have a stoichiometry of 1 or 2. In the presence of the nucleosomes, however,
479 we clearly observed an increased fraction of foci with a stoichiometry of 2 (**Supplementary**
480 **Figure 5.1b**). While in our experimental configuration a measured MCM stoichiometry of 2
481 within a diffraction-limited focus cannot distinguish an MCM double hexamer from two single
482 MCM hexamers, our results are consistent with previous work showing that a chromatinized
483 ARS1 origin favors the formation of the MCM/ORC (MO) intermediate complex and,
484 consequently, the loading of MCM double hexamers[16].
485
486

487 **MCM spatially constrained to a chromatinized origin on long timescales**

488 Our experimental tracking of MCM position over long incubation times shows that the
489 presence of nucleosomes spatially constrains MCM (**Figure 5e**). Does this spatial confinement
490 help to explain how the presence of origin-flanking nucleosomes favors pre-RC formation[11,
491 12]? Such spatial confinement will limit the diffusion of MCM single hexamers[15, 23] and thereby
492 reduce the likelihood of MCM double hexamer formation through the encounter of properly
493 oriented, diffusing MCM single hexamers[23]. Possibly, this favors MCM double hexamer
494 formation via the MO intermediate[16]. Future investigations will further investigate the
495 confinement of MCM by nucleosomes, as it could potentially contribute to the recycling of
496 licensing factors in cases of DNA replication stress, where reloading of factors is not possible.
497 replisome assembly at origins of replication flanked by nucleosomes.

498

499 **CONCLUSIONS**

500 Our findings provide new insights into the role of chromatin in DNA replication initiation. We
501 demonstrate that the presence of nucleosomes surrounding origins contributes to the loading
502 and subsequent spatial constraint of MCM hexamers there, which likely favors subsequent
503 CMG formation and the initiation of DNA replication at replication origins. Future
504 investigation will focus on the quantification of these downstream events. This research will
505 additionally open up new avenues to further explore the role of chromatin in origin firing and
506 the mechanisms of chromatin replication.

507

508 **METHODS**

509 Biological Materials

510 ***Protein purification and labeling***

511 **Histone octamers:** Plasmids pCDFduet.H2A-H2B and pET-Duet.H3-H4, expressing *S.*
512 *cerevisiae* histones H2A, H2B, H3 and H4 were kindly provided by Dr. Martin Singleton (Francis
513 Crick Institute, London). Lysine 120 of H2A was changed to cysteine by site-directed
514 mutagenesis to facilitate fluorescent labeling. These histones were co-expressed in
515 *Escherichia coli* strain BL21-codonplus-DE3-RIL (Agilent), and the histone octamer with the
516 K120>C mutation in histone H2A was purified according to Ref[33]. Cells were grown to a density
517 with an OD^{600} of 0.3-0.5, and expression of the histones was induced with 400 µM isopropyl
518 1-thio-ß-D-galactopyranoside (Santa Cruz Biotechnology Inc) for 16 h at 17°C while shaking at
519 180 rpm. Cells were lysed by sonication in a Qsonica Q500 sonicator for 2 min with cycles of
520 5 s on and 5 s off and an amplitude of 40%, in histone lysis buffer (0.5 M NaCl, 20 mM Tris-HCl
521 pH 8, 0.1 mM EDTA, 1 mM DTT, 0.3 mM PMSF, and protease cOmplete inhibitor). Supernatant
522 containing the histone octamers was purified on a 5 mL Hi-Trap Heparin column (Cytiva) and
523 eluted with a gradient of 0.5–2 M NaCl in 20 mM Tris-HCl pH 8, 0.1 mM EDTA, 1 mM DTT.
524 Peak fractions were analyzed on a 12% SDS-PAGE, and octamer-containing fractions were
525 further purified on a Superdex 200 increase (Cytiva) using histone GF buffer (2 M NaCl, 20
526 mM Tris-HCl pH 8, 0.1 mM EDTA, and 1 mM DTT). Peak fractions were analyzed on a 12% SDS-
527 PAGE gel, and fractions containing histone octamers were pooled and concentrated in an
528 Amicon Ultra-4 Ultracell 30kDa centrifugal filter (Merck-Millipore #UFC803024). The protein
529 concentration was determined with Bio-Rad Protein Assay Dye Reagent (Bio-Rad # 5000006).

530

531 **Cdc6**: *S. cerevisiae* Cdc6 protein expression was induced in BL21-CodonPlus(DE3)-RIL cells
532 (Agilent #230245) transformed with pGEX-6P-1 wt GST-cdc6 using 400 µM IPTG for 16 h at 16
533 °C. Cells were harvested in Cdc6 lysis buffer (50 mM K_XPO_4 pH 7.6, 150 mM KOAc, 5 mM $MgCl_2$,
534 1% Triton X-100, 2 mM ATP, cOmplete™ EDTA-free Protease Inhibitors (Sigma-Aldrich
535 #5056489001), and 1 mM DTT) and sonicated in a Qsonica Q500 sonicator for 2 min with
536 cycles of 5 s and 5 s off and an amplitude of 40%. After centrifugation, Cdc6 protein was
537 purified from the supernatant by incubating for 1 h at 4 ºC with glutathione beads Fastflow
538 (GE Healthcare #17-5132-02). The beads were washed 20 times with 5 ml Cdc6 lysis buffer,
539 and Cdc6 was released from the beads by digestion with Precision protease (GE Healthcare
540 #27-0843-01) at 4 ºC for 16 h. Subsequently, the Cdc6 eluate was diluted with Cdc6 dilution
541 buffer (50 mM K_XPO_4 pH 7.6, 5 mM $MgCl_2$, 0.1% Triton X-100, 2 mM ATP, and 1 mM DTT) to a
542 final KOAc concentration of 75 mM and incubated with hydroxyapatite Bio gel HTP (Bio-Rad
543 #130-0402) for 45 min at 4 ºC. The beads were washed five times with Cdc6 wash buffer (50
544 mM K_XPO_4 pH 7.6, 75 mM KOAc, 5 mM $MgCl_2$, 0.1% Triton X-100, 2 mM ATP, and 1 mM DTT),
545 and then washed five times with Cdc6 rinse buffer (50 mM K_XPO_4 pH 7.6, 150 mM KOAc, 5
546 mM $MgCl_2$, 15% glycerol, 0.1% Triton X-100, and 1 mM DTT). Next, Cdc6 was eluted from the
547 column in 1-ml fractions with Cdc6 elution buffer (50 mM KXPO4 pH 7.6, 400 mM KOAc, 5
548 mM $MgCl_2$, 15% glycerol, 0.1% Triton X-100, and 1 mM DTT). Finally, fractions containing Cdc6
549 were pooled, dialyzed twice for 1 h against Cdc6 dialysis buffer (25 mM HEPES-KOH pH 7.6,
550 100 mM KOAc, 10 mM MgOAc, 10% glycerol, and 0.02% NP40 substitute) in a 10 kDa cut off
551 Slide-A-Lyzer Cassette (Thermo Scientific #66380), and concentrated in an Amicon Ultra-4
552 Ultracell 30kDa centrifugal filter (Merck-Millipore #UFC803024). Aliquots were snap frozen
553 and stored at -80 ºC. The protein concentration was determined with Bio-Rad Protein Assay
554 Dye Reagent (Bio-rad # 5000006).

555

556 **ORC and Halo-tagged ORC:** ORC complex with a CBP-TEV tag on orc1 was purified from *S.*
557 *cerevisiae* strain ySDORC, and ORC complex with a CBP-TEV-Halo tag on orc3 was purified
558 from strain yTL158. Cells were seeded at a density of $2*10^7$ cells per ml in YP medium (1%
559 yeast extract and 2% peptone), supplemented with 2% raffinose and grown at 30 ^oC and 180
560 rpm until a density of $3\text{-}5*10^7$ cells/ml was reached. Then cells were arrested in G1 by adding
561 100 ng/ml α-mating factor (Tebu-Bio #089AS-60221-5) for 3 h followed by the addition of 2%
562 galactose for 3 h to induce the expression of ORC. Cells were harvested by centrifugation and
563 washed with ORC lysis buffer (25 mM HEPES-KOH pH 7.6, 0.05% NP-40 substitute, 10%
564 glycerol, 0.1 M KCl, and 1 mM DTT). After centrifugation, cells were suspended in ORC lysis
565 buffer supplemented with protease inhibitors (cOmplete^{TM} EDTA-free Protease Inhibitors
566 (Sigma-Aldrich #5056489001) and 0.3 mM PMSF) and dropped into liquid nitrogen. The frozen
567 droplets were ground in a freezer mill (6875 SPEX) for 6 cycles (run time 2 min and cool time
568 1 min with a rate of 15 cps), and the resulting powder was suspended in ORC lysis buffer
569 supplemented with protease inhibitors. The lysate was cleared in a Beckman-Coulter
570 ultracentrifuge (type Optima L90K with rotor TI45) for 1 h at 235.000 g at 4 ^oC. The cleared
571 lysate was supplemented with $CaCl_2$ to a final concentration of 2 mM and with KCl to a final
572 concentration of 0.3 M and then incubated for 1 h at 4 ^oC with washed Sepharose 4B
573 Calmodulin beads (GE Healthcare #17-0529-01) in a spinning rotor. The beads were washed
574 20 times with 5 ml ORC binding buffer (25 mM HEPES-KOH pH 7.6, 0.05% NP-40 substitute,
575 10% glycerol, 0.3 M KCl, 2 mM $CaCl_2$, and 1 mM DTT), and the protein complex was eluted
576 from the beads with ORC elution buffer (25 mM HEPES-KOH pH 7.6, 0.05% NP-40 substitute,
577 10% glycerol, 0.3 M KCl, 2 mM EDTA, 2 mM EGTA, and 1 mM DTT). ORC-containing fractions
578 were pooled, concentrated in an Amicon Ultra-4 Ultracell 30kDa centrifugal filter (Merck-

579 Millipore #UFC803024), and applied to a Superose 6 increase 10/300 GL column (GE
580 Healthcare #29-0915-96) equilibrated in ORC GF buffer (25 mM HEPES-KOH pH 7.6, 0.05% NP-
581 40 substitute, 10% glycerol, 0.15 M KCl, and 1 mM DTT). Peak fractions were pooled and
582 concentrated in an Amicon Ultra-4 Ultracell 30kDa centrifugal filter (Merck-Millipore
583 #UFC803024). Aliquots were snap frozen and stored at -80°C. The protein concentration was
584 determined with Bio-Rad Protein Assay Dye Reagent (Bio-Rad # 5000006).
585
586 **Mcm2-7/Cdt1 and Halo-tagged Mcm2-7/Cdt1**: Mcm2-7/Cdt1 complex with a CBP-TEV tag on
587 mcm3 was purified from *S. cerevisiae* strain yAM33, and Mcm2-7/Cdt1 complex with a CBP-
588 TEV-Halo tag on mcm3 was purified from strain yTL001. Cells were grown, and Mcm2-7/Cdt1
589 expression was induced as described for ORC. Cells were harvested by centrifugation and
590 washed with MCM lysis buffer (45 mM HEPES-KOH pH 7.6, 0.02% NP-40 substitute, 10%
591 glycerol, 100 mM KOAc, 5 mM MgOAc, and 1 mM DTT). After centrifugation, cells were
592 suspended in MCM lysis buffer supplemented with protease inhibitors (cOmplete^{TM} EDTA-
593 free Protease Inhibitors (Sigma-Aldrich #5056489001) and 0.3 mM PMSF) and dropped into
594 liquid nitrogen. The frozen droplets were ground in a freezer mill (6875 SPEX) for 6 cycles (run
595 time 2 min and cool time 1 min at a rate of 15 cps), and the resulting powder was suspended
596 in MCM lysis buffer supplemented with protease inhibitors. The lysate was cleared in a
597 Beckman-Coulter ultracentrifuge (type Optima L90K with rotor TI45) for 1 h at 235.000 g and
598 4 ^{o}C. The cleared lysate was supplemented with $CaCl_2$ to a final concentration of 2 mM and
599 then incubated for 1 h at 4 ^{o}C with washed Sepharose 4B Calmodulin beads (GE Healthcare
600 #17-0529-01) in a spinning rotor. The beads were washed 20 times with 5 ml MCM binding
601 buffer (45 mM HEPES-KOH pH 7.6, 0.02% NP-40 substitute, 10% glycerol, 100 mM KOAc, 5
602 mM MgOAc, 2 mM $CaCl_2$, and 1 mM DTT), and the protein complex was eluted from the beads

603 with MCM elution buffer (45 mM HEPES-KOH pH 7.6, 0.02% NP-40 substitute, 10% glycerol,
604 100 mM KOAc, 5 mM MgOAc, 1 mM EDTA, 2 mM EGTA, and 1 mM DTT). Mcm2-7/Cdt1-
605 containing fractions were pooled, concentrated in an Amicon Ultra-4 Ultracell 30kDa
606 centrifugal filter (Merck-Millipore #UFC803024), and applied to a Superose 6 increase 10/300
607 GL column (GE Healthcare #29-0915-96) equilibrated in MCM GF buffer (45 mM HEPES-KOH
608 pH 7.6, 0.02% NP-40 substitute, 10% glycerol, 100 mM KOAc, 5 mM MgOAc, and 1 mM DTT).
609 Peak fractions were pooled and concentrated in an Amicon Ultra-4 Ultracell 30kDa centrifugal
610 filter (Merck-Millipore #UFC803024). Aliquots were snap frozen and stored at -80 ^{o}C. Protein
611 concentration was determined with Bio-Rad Protein Assay Dye Reagent (Bio-Rad # 5000006).
612
613 **dCas9-Halo**: Halo-tagged dCas9 protein expression was induced in BL21-CodonPlus(DE3)-RIL
614 cells (Agilent #230245) transformed with pET302-6His-dCas9-halo (Addgene #72269) using
615 400 µM IPTG for 16 h at 16 °C. Cells were harvested in dCas9 lysis buffer (50 mM Na_xPO_4 pH
616 7.0, 300 mM NaCl and protease inhibitors (cOmplete^{TM} EDTA-free Protease Inhibitors (Sigma-
617 Aldrich #5056489001) plus 0.3 mM PMSF)) and sonicated in an Qsonica Q500 sonicator for 2
618 min with cycles of 5 s on and 5 s off and an amplitude of 40%. After centrifugation, dCas9-
619 Halo protein was purified from the supernatant by incubating for 2 h at 4 ^{o}C with Ni-NTA
620 agarose (Qiagen #30210). The beads were washed 10 times with 5 ml dCas9 wash buffer I (50
621 mM Na_xPO_4 pH 7.0 and 300 mM NaCl) and 3 times with dCas9 wash buffer II (50 mM Na_xPO4
622 pH 7.0, 300 mM NaCl, and 20 mM Imidazole pH 7.6), and dCas9-Halo was eluted from the
623 agarose beads with dCas9 elution buffer (50 mM Na_xPO_4 pH 7.0, 300 mM NaCl, and 150 mM
624 Imidazole pH 7.6). Subsequently, dCas9-Halo eluate was dialyzed twice for 1 h against dCas9-
625 dialysis buffer (50 mM HEPES-KOH pH 7.6, 100 mM KCl, and 1 mM DTT) in a 10kDa cut off
626 Slide-A-Lyzer Cassette (Thermo Scientific #66380) and applied to a Hi Trap SP HP column (GE

627 Healthcare #17-1151-01) equilibrated with dCas9 dialysis buffer. The dCas9-Halo protein was
628 eluted from the column with dialysis buffer with a KCl gradient ranging from 100 mM up to 1
629 M. The dCas9-Halo-containing fractions were pooled, concentrated in an Amicon Ultra-4
630 Ultracell 30kDa centrifugal filter (Merck-Millipore #UFC803024), and applied to a Superdex
631 200 increase 10/300 GL column (GE Healthcare #28-9909-44) equilibrated in cas9 GF buffer
632 (50 mM HEPES-KOH pH 7.6, 150 mM KCl, and 1 mM DTT). Peak fractions were pooled and
633 concentrated in an Amicon Ultra-4 Ultracell 30kDa centrifugal filter (Merck-Millipore
634 #UFC803024). Aliquots were snap frozen and stored at -80 ^{o}C. The protein concentration was
635 determined with Bio-Rad Protein Assay Dye Reagent (Bio-Rad # 5000006).
636
637 **dCas9-Cys**: dCas9-Cys protein expression was induced in BL21-CodonPlus(DE3)-RIL cells
638 (Agilent #230245) transformed with plasmid 10xHis-MBP-TEV-S. pyogenes dCas9 M1C D10A
639 C80S H840A C574S (Addgene #60815) with 400 µM IPTG for 5 h at 20 °C. Cells were harvested
640 in dCas9-cys lysis buffer (20 mM Tris-HCl pH 8.0, 500 mM NaCl, 1mM DTT, and protease
641 inhibitors (cOmpleteTM EDTA-free Protease Inhibitors (Sigma-Aldrich #5056489001) plus 0.3
642 mM PMSF)) and sonicated in an Qsonica Q500 sonicator for 2 min with cycles of 5 s on and 5
643 s off and an amplitude of 40%. After centrifugation, dCas9-Cys protein was purified from the
644 supernatant by incubating for 2 h at 4 °C with Ni-NTA agarose (Qiagen #30210). The beads
645 were washed 10 times with 5 ml dCas9-Cys wash buffer (20 mM Tris-HCl pH 8.0, 250 mM
646 NaCl, 20mM imidazole pH 7.6), and dCas9-Cys was eluted from the agarose beads with dCas9-
647 Cys elution buffer (20 mM Tris-HCl pH 8.0, 250 mM NaCl, 150 mM imidazole pH 7.6).
648 Subsequently, dCas9-Cys eluate was dialyzed twice for 1 h against dCas9-Cys-dialysis buffer
649 (20 mM HEPES-KOH pH 7.6, 150 mM KCl, and 1 mM DTT) in a 10 kDa cut off Slide-A-Lyzer
650 Cassette (Thermo Scientific #66380) and applied to a Hi Trap SP HP column (GE Healthcare

651 #17-1151-01) equilibrated with dCas9-Cys dialysis buffer. The dCas9-Cys protein was eluted
652 from the column with dCas9-Cys dialysis buffer with a KCl gradient ranging from 100 mM up
653 to 1 M. The dCas9-Cys-containing fractions were pooled, concentrated in an Amicon Ultra-4
654 Ultracell 30kDa centrifugal filter (Merck-Millipore #UFC803024), and applied to a Superdex
655 200 increase 10/300 GL column (GE Healthcare #28-9909-44) equilibrated in cas9-Cys GF
656 buffer (20 mM HEPES-KOH pH 7.6, 150 mM KCl, and 1 mM DTT). Peak fractions were pooled
657 and concentrated in an Amicon Ultra-4 Ultracell 30 kDa centrifugal filter (Merck-Millipore
658 #UFC803024). Aliquots were snap frozen and stored at -80 ^{o}C. The protein concentration was
659 determined with Bio-Rad Protein Assay Dye Reagent (Bio-Rad # 5000006).
660
661 ***Protein labeling***
662 Strains: To create Halo-tagged mcm3, the StuI and XmaI restriction sites in plasmid pENTR4-
663 HaloTag (Addgene #W876-1) were changed into a silent mutation following standard cloning
664 techniques using primers TL-019-TL-020 and TL-023-TL-024. The sequence was verified by
665 sequencing using primers TL-021-TL-022. Then the HaloTag fragment was amplified from the
666 mutated pENTR4-HaloTag by PCR with primers TL-025 and TL-026, which were extended with
667 an XmaI site. This amplified HaloTag was digested with XmaI, gel-purified, and ligated into
668 plasmid pRS306 CBP-TEV-mcm3-gal1-10 mcm2, which was digested with SgrAI and
669 dephosphorylated with CIP, resulting in plasmid pRS306 CBP-TEV-mhalo-mcm3-gal1-10
670 mcm2. Proper integration of the HaloTag was confirmed by sequencing with primers (see
671 Supplementary Table 1) TL-001, TL-002, TL-027, and TL-028. Yeast strain yTL001, which
672 expresses MCM with a Halo-tagged mcm3, was created by linearizing plasmid pRS306 CBP-
673 TEV-mhalo-mcm3-gal1-10-mcm2 with StuI and transforming it into yeast strain yJF21, which
674 expresses Mcm4-7 and Cdt1 upon induction with galactose.

675 To create an ORC complex with a halo-tagged orc3, the CBP-TEV sites was removed from
676 plasmid pRS306 orc1-gal1-10-orc2 through Gibson assembly (NEB #E2611L) using primers TL-
677 441, TL-443, and TL-447. The sequence for the coding region of orc1 and orc2 was confirmed
678 by sequencing using primers TL-084, TL-087, TL-119, and TL-136. Yeast strain yTL151, which
679 expresses orc1, 2, 5, and 6 from a galactose-inducible promoter, was created by linearizing
680 plasmid pRS306 orcl-gal1-10-orc2 v2 delta CBP-TEV with StuI and transforming it into yeast
681 strain yTL070, which contains an inducible expression plasmid for orc5 and orc6.
682
683 Plasmid pRS303 CBP-TEV-halo-orc3 gal1-10 orc4 was generated by cloning the CBP-TEV-halo
684 sequence from plasmid pRS306-CBP-TEV-halo-Pri1 -Gal1-10 Pri2 into plasmid pRS303-orc3-
685 Gal1-10 orc4 through Gibson assembly (NEB #E2611L) using primers TL-446, TL-447, TL-472,
686 and TL-473). The sequence of CBP-TEV-halo-orc3 and orc4 was verified by sequencing using
687 primers TL-063, TL-064, TL-449, and TL-470. Yeast strain yTL158, which expresses ORC with a
688 halo-tagged orc3, was created by linearizing plasmid pRS303-CBP-TEV-halo-orc3-Gal1-10 orc4
689 with NheI and transforming it into yeast strain yTL151, which contains inducible expression
690 plasmids for orc1, orc2, orc5, and orc6.
691
692 Labeling reactions: Proteins with HaloTag were labeled with JF646-HaloTag ligand (Promega
693 # GA1120) by incubating the proteins with a tenfold excess of dye on ice for 0.5-1 h in the
694 presence of 1 mM ATP. Free dye was removed by gel filtration (Superose 6 increase 10/300),
695 and the labeling efficiency was determined to be 75% and 80% for JF646-ORC and JF646-
696 MCM, respectively, after estimating protein and fluorophore concentrations relative to
697 known standards. Accordingly, we cannot exclude the possibility that ~25% and 20% of the

698 observed single ORC or single MCM populations may have been partially labeled double ORC
699 and double MCM hexamers.
700
701 Proteins with a single cysteine were labeled with Alexa Fluor 488 C5 Maleimide (Invitrogen #
702 A10254) by incubating the proteins with a tenfold excess of dye on ice for 2 h at pH 7 in the
703 absence of DTT. Free dye was removed by gel filtration (Superose 6 increase 10/300), for
704 dCas9, or by dialysis with 2 M NaCl, 20 mM Tris-HCl pH 8, and 1 mM DTT followed by spin
705 column chromatography (Zeba 7k MWCO) for histone octamers. Labeling efficiency was
706 determined to be 81% for AF488-H2A, after estimating protein and fluorophore
707 concentrations relative to known standards.
708
709 ***DNA substrates for single-molecule imaging***
710 To generate a biotinylated 10.4 kbp DNA molecule containing ARS1 or mutated origin flanked
711 by nucleosome positioning sequences, we ligated three different DNA fragments prepared by
712 PCR. The left biotinylated arm with 6.6 kbp was amplified from plasmid pDRM1 (a kind gift
713 from Daniel Ramírez-Montero) by PCR using primers HS_BN47 and HS_BN48 (ELLA Biotech)
714 with Platinum SuperFi II DNA Polymerase (Thermo Scientific #12361010). The right
715 biotinylated arm with 3.3 kbp was amplified as above from plasmid pDRM1 using primers
716 HS_BN45 and HS_BN46 (ELLA Biotech). Biotinylated PCR products were purified by standard
717 phenol-chloroform extraction, precipitated with ethanol and digested overnight with BsaI
718 (NEB # R3733S). Digested biotinylated arms were purified by spin column chromatography
719 using MicroSpin S-400 HR (Amersham # 27514001).
720

721 To generate a DNA fragment compatible for ligation containing ARS1 or mutated origin
722 flanked by nucleosome positioning sequences, we first prepared template plasmids
723 containing the origins. Plasmid template TL20-042 with ARS1 origin site flanked by 601 and a
724 603 nucleosome positioning sites[34], was prepared by cloning into MluI-digested and Antarctic
725 - dephosphorylated plasmid pSupercos1-lambda1,2[35] of PCR fragment amplified from gBlock
726 gene fragment (IDT) pTL013[16] using primers TL-817 and TL-818, digested with AscI. Plasmid
727 template TL22-072 with mutated ORC binding-site, was prepared by one-step cloning using
728 NEBuilder HiFi reaction (NEB # E5520S) into plasmid pIA146[36] linearized with HindIII (NEB #
729 R3104S) of the fragment containing the mutated origin amplified from gBlock gene fragment
730 (IDT)pGC218[23] with primers TL-961 and TL-964, and the fragments containing the nucleosome
731 positioning sites 601 and 603 independently amplified from gBlock gene fragment
732 (IDT)pTL013[16] with primers TL-958 – TL-959 and TL-962 – TL-963, respectively.
733
734 PCR fragments containing the origins and compatible BsaI ends were prepared from TL20-042
735 and TL22-072 by PCR using primers HS_BN23NPb and HS_BN26NPb (ELLA Biotech). PCR
736 products were purified by standard phenol-chloroform extraction, precipitated with ethanol,
737 digested overnight with BsaI (NEB # R3733S) and gel-purified.
738
739 Nucleosome assembly was carried out using salt gradient dialysis[37]. Fluorescently labeled
740 histone octamers were mixed with DNA in High Salt Buffer (10 mM Tris pH 7.5, 2 M NaCl, 1
741 mM EDTA, 1 mM DTT). Samples were dialyzed for 18 h against 400 ml of High Salt Buffer and
742 gradually supplemented with 2 L of Low Salt Buffer (10 mM Tris pH 7.6, 250 mM NaCl, 1 mM
743 EDTA, 1 mM DTT). A final dialysis step for 1 h was performed into Zero Salt Buffer (20 mM Tris
744 pH 7.5, 1 mM EDTA, 1 mM DTT). Fluorescently labeled histone octamer concentrations were

745 optimized by small-scale titration and nucleosomes checked by 5% native PAGE. To test that
746 the origin sequence is free of nucleosomes and accessible to ORC and MCM, the
747 chromatinized construct were digested with Pst I (NEB#R0140S) and fragment size checked
748 by 5% native PAGE. PCRs fragments with BsaI compatible ends were ligated to the
749 chromatinized origins with T4 ligase overnight at 16 ^{o}C. The concentration of nucleosomes is
750 maintained above 20 μg/ml to avoid dissociation due to dilution[38] using commercial
751 nucleosomes (Epicypher #160009). Final constructs were dialyzed overnight against 25 mM
752 HEPES pH 7.6.
753
754 Bulk Assays and Single-Molecule Experiments
755 ***MCM recruitment and loading reactions in bulk to test protein activity***
756 Loading assays were carried out as follows: 50 nM ORC (or JF646-ORC), 50 nM Cdc6 and 100
757 nM Mcm2-7/Cdt1 (or JF646-Mcm2-7/Cdt1) were incubated with 300 ng DNA substrate (5.8
758 kbp circular bead-bound ARS1-containing pSK (+)-based plasmid[39]) coupled to magnetic
759 beads for 30 min at 30 °C with mixing at 1250 rpm in 40 µl reaction buffer (25 mM HEPES-
760 KOH pH 7.6, 10 mM MgOAc, 100 mM KOAc, 0.02% NP40, 5% glycerol, 1 mM DTT, and 5 mM
761 ATP or ATPγS). Beads were then washed either with high salt wash buffer (45 mM HEPES-KOH
762 pH 7.6, 5 mM MgOAc, 0.5 M NaCl, 0.02% NP-40, 10% glycerol, 1 mM EDTA, and 1 mM EGTA)
763 followed by low salt wash buffer (45 mM HEPES-KOH pH 7.6, 5 mM MgOAc, 0.3 M KOAc,
764 0.02% NP-40, 10% glycerol, 1mM EDTA, and 1 mM EGTA), or only treated with low salt wash
765 buffer. Finally, beads were resuspended in 10 µl elution buffer (45 mM HEPES-KOH pH 7.6, 5
766 mM MgOAc, 0.3 M KOAc, 10% glycerol, and 2 mM $CaCl_2$), and DNA-bound proteins were
767 released by MNase treatment (2 min 30° with 700 units of MNase NEB # M0247S) and
768 analyzed by gel electrophoresis[40].

769

770 ***Single-molecule instrumentation and visualization***

771 A hybrid instrument combining optical tweezers and confocal microscopy was used to
772 visualize the binding of DNA and protein at the single-molecule level (Q-Trap, LUMICKS) as
773 described[7, 15] with the following variations. The instrument makes use of a customer designed
774 microfluidic flow cell with three inlets for injection of reaction buffers from the left and up to
775 six inlets that are introduced orthogonally and can be used as protein reservoirs or buffer
776 exchange locations in a temperature-controlled environment. Syringes and tubing connected
777 to the flow cell were passivated, together with the flow cell itself, with 1 mg/ml BSA followed
778 by 0.5% Pluronic F-127 (Sigma), each incubated for at least 30 min. Next, 20 pM of the
779 biotinylated DNA, containing either a functional origin of replication or a mutated origin,
780 chromatinized or not, was injected into one of the three laminar-flow-separated channels.
781 Individual DNA molecules were trapped between two 1.76 µm diameter streptavidin-coated
782 polystyrene beads (Spherotech) initially injected into a separate channel.

783

784 In all measurements, the stiffness of both optical traps was set to 0.3 pN/nm[41, 42] The
785 tethering of individual DNA molecules was verified by analysis of the force-extension curve
786 obtained for each DNA molecule[43] that was used for protein visualization. During fluorescence
787 measurements, the DNA was held at a constant tension of 2 pN and the flow was turned off,
788 unless otherwise specified. The AF488 and JF646 dyes were illuminated with two laser lines
789 at 488 nm (2 µW) and 638 nm (7 µW), respectively, and the fluorescence from the dyes was
790 detected on a single photon counting detector. Two-dimensional confocal scans were
791 performed over an area of 90 x 18 pixels, which encompasses the DNA held at a force of 2 pN

792 and the edges of both beads. The pixel size was set to 50x50 nm^2, and the illumination time
793 per pixel was set to 0.1 ms.
794
795 ***Protein concentrations and buffers in single-molecule experiments***
796 Incubation and visualization of DNA-protein interactions in the flow cell were performed at
797 30 °C. ORC binding was conducted in reaction buffer (RB) containing 25 mM HEPES-KOH pH
798 7.6, 100 mM potassium glutamate, 10 mM magnesium acetate, 100 µg/mL BSA, 1 mM DTT,
799 0.01% NP-40-S, 10% glycerol, 5 mM ATP, with 10 nM Cdc6 and 5 nM JF646-ORC. To reduce
800 the rate of photobleaching, we add 2 mM 1,3,5,7 cyclooctatetraene, 2 mM 4-
801 nitrobenzylalchohol and 2 mM TROLOX.
802
803 Preparation of DNA-protein complexes in bulk for subsequent visualization in the flow cell
804 was done as follows: 5 nM ORC was incubated with 1 nM 10.4 kbp biotinylated DNA
805 (chromatinized or not) at 30 °C while mixing at 800 rpm in RB with 5 mM ATP. After 5 min, 10
806 nM Cdc6 was added to the reaction and incubated for a further 5 min. Then, 80 nM
807 MCM/Cdt1 was added, bringing the total reaction volume to 50 µl. Following a 30 min
808 incubation, samples were diluted 15 x in RB and injected into the microfluidic chip. ORC-Cdc6
809 DNA complexes were assembled in the same conditions while omitting Mcm2-7/Cdt1.
810
811 Data analysis
812 ***Particle localization in 2D scans***
813 We use the scikit-image (v0.16.2) implementation of a Laplacian of Gaussian (LoG) spot
814 detector. The detection radius r_{LoG} is set to 6.5 pixels (312 nm) for the red channel and 5 pixels
815 (240 nm) for the blue channel; the LoG sigma parameter is given by $\sigma_{LoG} = r_{LoG} / \sqrt{2}$. We set

816 the detection threshold to 0.2 ADU/pixel for the red channel and 0.3 ADU/pixel for the blue
817 channel. For subpixel localization, detected spots are projected onto the x- and y-axes and
818 then fitted with Gaussian profiles.
819
820 ***Particle tracking***
821 The spots are tracked through subsequent frames using our own implementation of the
822 Linear Assignment Problem method[44]. We used a maximum spot linking distance of 10 pixels
823 (480 nm) for the red channel and 4 pixels (192 nm) for the blue channel using a maximum
824 frame gap of 3 frames (1.8 seconds) without splitting. The LAP is solved with the scipy (v1.6.1)
825 linear sum assignment optimizer[45]. Two spots are considered colocalized if they are on
826 average less than 4 pixels (200 nm) apart over the first 5 frames; spot intensities are calculated
827 by taking the total ADU count within the detection radius.
828
829 ***Location calibration***
830 Using a reference dCas9 dataset, we map the location of two known DNA sequences onto
831 pixel coordinates, relative to the left bead (whose coordinate is given in microns by the C-
832 Trap metadata, as measured in the brightfield view). With these pixel coordinates we
833 calculate the inverse transformation, from pixel coordinate to DNA sequence location in base
834 pairs, giving us a brightfield-to-confocal offset value (4.5 pixels) and a pixel size value (48 nm
835 per pixel).
836
837 ***Fluorophore intensity calibration***
838 The reference dCas9 dataset is also used for fluorophore intensity calibration. Foci with one
839 bleaching step are used to make a distribution of intensity bleaching steps and calculate the

840 mean $\mu_{\Delta I}$ and standard deviation $\sigma_{\Delta I}$ of that distribution. The minimum bleaching step size,
841 which is needed for stoichiometry determination of further experiments, is set to $\Delta I_{min} \leq \mu_{\Delta I}$ -
842 $2\ \sigma_{\Delta I}$ in order to capture at least 95% of all bleaching events. The measured values of $\mu_{\Delta I}$ and
843 $\sigma_{\Delta I}$ for each color are given in **Table 1**.
844

Fluorophore	Signal	$\mu_{\Delta I}$ (ADU)	$\sigma_{\Delta I}$(ADU)	ΔI_{min} (ADU)	N_{foci}
AF488	blue	41.6	9.8	20	43
JF646	red	176.7	22	75	14

845 **Table 1.** Fluorophore properties, calibrated using dCas9 data.
846
847 ***Stoichiometry determination***
848 To determine the number of fluorophores present within each detected spot, we perform
849 photobleaching step counting using Change-Point Analysis (CPA). We use the ruptures
850 (v1.1.6) [46] implementation with an L2 cost function to detect mean-shifts in the signal. The
851 minimum segment length is set to 2 and the penalty is set to ΔI_{min}^2. If any steps larger than
852 ΔI_{min} are present after the fit, the smallest steps are combined together ("pruned") until only
853 steps larger than ΔI_{min} are left.
854
855 ***Data filtering***
856 The resulting data table of traces with number of fluorescent proteins per spot was filtered in
857 order to reduce noise, outliers, and data that is not suitable for further motion analysis:
858 Diffraction-limited spots containing more than 5 fluorescent proteins, likely aggregates, are
859 filtered out.

860 Any traces starting or ending within 1 kbp from a bead are filtered out to prevent any proteins
861 likely stuck to a bead from entering the dataset.
862 Any traces starting after frame 5 are also filtered away because we do not expect any
863 fluorescent protein to land on the DNA during the scan.
864 Finally, only traces with a length of 5 frames or more are retained for diffusion analysis.
865
866 ***Spatial distribution analysis***
867 In spatial distribution plots we show the average position of the spot over the first three
868 frames. The bin size of the histogram is set to 670 bp to be close to (but slightly larger than)
869 the diffraction limit. Together with the binned data we plot the kernel density estimation of
870 the data with a bandwidth that is equivalent to half of the bin size in the histogram (335 bp)
871 and is higher than the localization error in the imaging conditions (100 bp).
872
873 ***Motion analysis***
874 We analyzed the mean squared displacement (MSD) of individual tracked foci as a function
875 of the delay time between frames as previously described[15, 47]. We employ a Gaussian Mixture
876 Model to fit the distribution of log(D) in the data set without a chromatinized origin, in order
877 to differentiate between different kinetic populations. We assess the statistical preference
878 for either a two-state or single-state model using the Bayesian Information Criterion, and the
879 two-state model is favored. We identified these states as a static population (D_{slow} = 0.0049 ±
880 0.0028 kbp^2 s^{-1} (mean ± SEM)) and a diffusive population (D_{fast} = 0.152 ± 0.023 kbp^2 s^{-1}). The
881 means of these subpopulations are imposed in the fits to the other datasets.
882

883 We calculated the mean, variance, and standard error (*m, var, SEM*) of the ith diffusion

884 coefficient distribution from the fitted lognormal parameters μ_i and σ_i according to:

885 $$m_i = e^{\ln(10)\mu_i + (\ln(10)\sigma_i)^2/2} \quad \text{(Eq. 1)}$$

886 $$var_i = e^{2\ln(10)\mu_i + (\ln(10)\sigma_i)^2/2}\left(e^{(\ln(10)\sigma_i)^2} - 1\right) \quad \text{(Eq. 2)}$$

887 $$SEM_i = \sqrt{\mathrm{var}_i/\mathrm{N}_i}, \quad \text{(Eq. 3)}$$

888 where the factors of log(*e*) and ln(10) account for our use of base 10, and N_i is the number of

889 values in the data set times the area of the ith fitted peak. It is worth noting that the

890 dependence of m_i on both μ_i and σ_i yields mean diffusion constants larger than might be

891 inferred by simply computing 10^{μ_i}.

892

893 ***Probability model for H2A stoichiometry distributions***

894 We formulate a probability model for H2A stoichiometry based on three probabilistic

895 quantities, the site occupation probability P_{occ}, the H2A binding probability P_{H2A}, and the

896 labeling efficiency P_{lab}.

897

898 The probability of having 0, 1, or 2 occupied sites (N_{occ}) on the DNA depends on the site

899 occupation probability (P_{occ}) following the binomial distribution:

900 $$\begin{aligned} P(N_{occ} = 0) &= (1 - P_{occ})^2 \\ P(N_{occ} = 1) &= 2P_{occ}(1 - P_{occ}) \\ P(N_{occ} = 2) &= P_{occ}^2 \end{aligned} \quad \text{(Eq. 4)}$$

901 An H2A-H2B dimer binds to the tetrasome with a probability of P_{H2A}. Again following the

902 binomial distribution, the probabilities of a tetrasome, hexasome and full nucleosome

903 forming are respectively:

$$P_{tet} = (1 - P_{H2A})^2$$

$$P_{hex} = 2P_{H2A}(1 - P_{H2A}) \qquad \text{(Eq. 5)}$$

$$P_{nuc} = P_{H2A}^2$$

Combining the two parts listed above yields the probabilities for encountering the possible numbers of H2A (N_{H2A}) on the DNA:

$$\begin{aligned} P(N_{H2A} = 1) &= P(N_{occ} = 1) \times P_{hex} + P(N_{occ} = 2) \times 2P_{tet}P_{hex} \\ P(N_{H2A} = 2) &= P(N_{occ} = 1) \times P_{nuc} + P(N_{occ} = 2) \times (P_{hex}^2 + 2P_{tet}P_{nuc}) \\ P(N_{H2A} = 3) &= P(N_{occ} = 2) \times 2P_{hex}P_{nuc} \\ P(N_{H2A} = 4) &= P(N_{occ} = 2) \times P_{nuc}^2 \end{aligned} \qquad \text{(Eq. 6)}$$

Finally, we need to take labeling efficiency P_{lab} into account. This gives us the probabilities for finding N_{vis} visible fluorophores in a diffraction-limited spot on the DNA:

$$\begin{aligned} P(N_{vis} = 1) &= P(N_{H2A} = 1) \times P_{lab} + P(N_{H2A} = 2) \times 2P_{lab}(1 - P_{lab}) + \\ &\quad P(N_{H2A} = 3) \times 3P_{lab}(1 - P_{lab})^2 + \\ &\quad P(N_{H2A} = 4) \times 4P_{lab}(1 - P_{lab})^3 \\ P(N_{vis} = 2) &= P(N_{H2A} = 2) \times P_{lab}^2 + P(N_{H2A} = 3) \times 3P_{lab}^2(1 - P_{lab}) + \\ &\quad P(N_{H2A} = 4) \times 6P_{lab}^2(1 - P_{lab})^2 \\ P(N_{vis} = 3) &= P(N_{H2A} = 3) \times P_{lab}^3 + P(N_{H2A} = 4) \times 4P_{lab}^3(1 - P_{lab}) \\ P(N_{vis} = 4) &= P(N_{H2A} = 4) \times P_{lab}^4 \end{aligned} \qquad \text{(Eq. 7)}$$

Force analysis

To quantify unwrapping of DNA from nucleosomes, we performed a transformation of force-distance curves to contour length space. The persistence length L_p and stretch modulus S of dsDNA in the measurement buffer were determined by pulling on bare dsDNA molecules to the overstretching regime at a constant pulling speed of 100 nm/s and fitting the force-distance curves using the extensible worm-like chain model[48]:

918 $$d = L_c\left[1 - \frac{1}{2}\left(\frac{k_B T}{F L_p}\right)^{\frac{1}{2}} + \frac{F}{S}\right], \qquad \text{(Eq. 8)}$$

919 where d is the distance between the two ends of the dsDNA, L_c is the DNA contour length, k_B
920 is Boltzmann constant, and F is the pulling force. The fitting results are L_p = 44.2 nm and S =
921 1421 pN.

922

923 The force-distance curves obtained by pulling on the chromatin sample were transformed to
924 contour length space by calculating the DNA contour length L_c using Eq. 9, an inversion of Eq.
925 8, and plotting L_c against pulling force applied to the chromatin:

926 $$L_c = \frac{1}{d}\left[1 - \frac{1}{2}\left(\frac{k_B T}{F L_p}\right)^{\frac{1}{2}} + \frac{F}{S}\right]. \qquad \text{(Eq. 9)}$$

927 This results in graphs with segments of constant L_c. CPA (again using the ruptures library with
928 an L2 cost function) was applied to the L_c-F plots to identify the plateaus and extract contour
929 length increments between the plateaus, which resulted from unwrapping of nucleosomes,
930 as well as the nucleosome unwrapping forces. This process follows the same steps as the
931 fluorophore bleaching step fitting analysis, but here we set the minimum step size to 10 nm,
932 after calibration with dsDNA.

933

934 ***Experiment automation***

935 To automate some of the C-trap measurements, we used the Lumicks Harbor experiment
936 automation scripts (https://harbor.lumicks.com/scripts) as a starting point; most notably,
937 Joep Vanlier's automation script for catching beads, fishing for DNA, and making force-
938 distance curves. We added the functionality to automatically acquire confocal images after
939 successfully trapping DNA.

940

941 ***Error determination***

942 To compute the statistical error in population, stoichiometry and diffusion plots, we use the
943 Wilson confidence interval. This is an improvement over the normal approximation for the
944 error of sample proportion, especially for a small number of trials[49]. We use the statsmodels
945 (Python) implementation for its calculation[50].

946

947 ***Figure schematics***

948 Figure schematics were generated using BioRender.com (Standard Academic License).

949

950 ***Data availability***

951 The data that support the findings of this study are available from the authors upon
952 reasonable request.

953

954 ***Code availability***

955 The analysis of the acquired data was performed using custom-written scripts in Python 3.8,
956 which are available upon request.

957

958 **REFERENCES**

959 1. Bellush JM, Whitehouse I. DNA replication through a chromatin environment. *Philos T*
960 *R Soc B* **372**, (2017).
961
962 2. Bell SP, Labib K. Chromosome Duplication in Saccharomyces cerevisiae. *Genetics* **203**,
963 1027-1067 (2016).
964
965 3. Bell SP, Stillman B. Atp-Dependent Recognition of Eukaryotic Origins of DNA-
966 Replication by a Multiprotein Complex. *Nature* **357**, 128-134 (1992).
967
968 4. Evrin C*, et al.* A double-hexameric MCM2-7 complex is loaded onto origin DNA during
969 licensing of eukaryotic DNA replication. *P Natl Acad Sci USA* **106**, 20240-20245 (2009).
970
971 5. Remus D, Beuron F, Tolun G, Griffith JD, Morris EP, Diffley JFX. Concerted Loading of
972 Mcm2-7 Double Hexamers around DNA during DNA Replication Origin Licensing. *Cell*
973 **139**, 719-730 (2009).
974
975 6. Douglas ME, Ali FA, Costa A, Diffley JFX. The mechanism of eukaryotic CMG helicase
976 activation. *Nature* **555**, 265-+ (2018).
977
978 7. Ramirez Montero D*, et al.* Nucleotide binding halts diffusion of the eukaryotic
979 replicative helicase during activation. *Nat Commun* **14**, 2082 (2023).
980
981 8. Yeeles JT, Deegan TD, Janska A, Early A, Diffley JF. Regulated eukaryotic DNA
982 replication origin firing with purified proteins. *Nature* **519**, 431-435 (2015).
983
984 9. Yeeles JTP, Janska A, Early A, Diffley JFX. How the Eukaryotic Replisome Achieves Rapid
985 and Efficient DNA Replication. *Mol Cell* **65**, 105-116 (2017).
986
987 10. Venditti P, Costanzo G, Negri R, Camilloni G. Abfi Contributes to the Chromatin
988 Organization of Saccharomyces-Cerevisiae Ars1 B-Domain. *Bba-Gene Struct Expr*
989 **1219**, 677-689 (1994).
990
991 11. Eaton ML, Galani K, Kang S, Bell SP, MacAlpine DM. Conserved nucleosome positioning
992 defines replication origins. *Gene Dev* **24**, 748-753 (2010).
993
994 12. Lipford JR, Bell SP. Nucleosomes positioned by ORC facilitate the initiation of DNA
995 replication. *Mol Cell* **7**, 21-30 (2001).
996
997 13. Chacin E*, et al.* Establishment and function of chromatin organization at replication
998 origins. *Nature*, (2023).
999
1000 14. Azmi IF*, et al.* Nucleosomes influence multiple steps during replication initiation. *Elife*
1001 **6**, (2017).
1002

1003 15. Sanchez H*, et al.* DNA replication origins retain mobile licensing proteins. *Nature*
1004 *Communications* **12**, (2021).
1005
1006 16. Miller TCR, Locke J, Greiwe JF, Diffley JFX, Costa A. Mechanism of head-to-head MCM
1007 double-hexamer formation revealed by cryo-EM. *Nature* **575**, 704-+ (2019).
1008
1009 17. Liachko I, Youngblood RA, Keich U, Dunham MJ. High-resolution mapping,
1010 characterization, and optimization of autonomously replicating sequences in yeast.
1011 *Genome Res* **23**, 698-704 (2013).
1012
1013 18. Andrews AJ, Chen X, Zevin A, Stargell LA, Luger K. The Histone Chaperone Nap1
1014 Promotes Nucleosome Assembly by Eliminating Nonnucleosomal Histone DNA
1015 Interactions. *Mol Cell* **37**, 834-842 (2010).
1016
1017 19. Brower-Toland BD, Smith CL, Yeh RC, Lis JT, Peterson CL, Wang MD. Mechanical
1018 disruption of individual nucleosomes reveals a reversible multistage release of DNA. *P*
1019 *Natl Acad Sci USA* **99**, 1960-1965 (2002).
1020
1021 20. Diaz-Celis C*, et al.* Assignment of structural transitions during mechanical unwrapping
1022 of nucleosomes and their disassembly products. *P Natl Acad Sci USA* **119**, (2022).
1023
1024 21. Mihardja S, Spakowitz AJ, Zhang YL, Bustamante C. Effect of force on
1025 mononucleosomal dynamics. *P Natl Acad Sci USA* **103**, 15871-15876 (2006).
1026
1027 22. Sheinin MY, Li M, Soltani M, Luger K, Wang MD. Torque modulates nucleosome
1028 stability and facilitates H2A/H2B dimer loss. *Nature Communications* **4**, (2013).
1029
1030 23. Coster G, Diffley JFX. Bidirectional eukaryotic DNA replication is established by quasi-
1031 symmetrical helicase loading (vol 357, pg 314, 2017). *Science* **357**, 314-318 (2017).
1032
1033 24. Li S, Wasserman MR, Yurieva O, Bai L, O'Donnell ME, Liu SX. Origin recognition complex
1034 harbors an intrinsic nucleosome remodeling activity. *P Natl Acad Sci USA* **119**, (2022).
1035
1036 25. Speck C, Stillman B. Cdc6 ATPase activity regulates ORC center dot Cdc6 stability and
1037 the selection of specific DNA sequences as origins of DNA replication. *J Biol Chem* **282**,
1038 11705-11714 (2007).
1039
1040 26. Li S, Wasserman MR, Yurieva O, Bai L, O'Donnell ME, Liu SX. Nucleosome-directed
1041 replication origin licensing independent of a consensus DNA sequence. *Nature*
1042 *Communications* **13**, (2022).
1043
1044 27. Devbhandari S, Jiang JQ, Kumar C, Whitehouse I, Remus D. Chromatin Constrains the
1045 Initiation and Elongation of DNA Replication. *Mol Cell* **65**, 131-141 (2017).
1046
1047 28. Marahrens Y, Stillman B. A Yeast Chromosomal Origin of DNA-Replication Defined by
1048 Multiple Functional Elements. *Science* **255**, 817-823 (1992).
1049

1050 29. De Ioannes P*, et al.* Structure and function of the Orc1 BAH-nucleosome complex.
1051 *Nature Communications* **10**, (2019).
1052
1053 30. Li NN*, et al.* Structure of the origin recognition complex bound to DNA replication
1054 origin. *Nature* **559**, 217-+ (2018).
1055
1056 31. Petryk N*, et al.* MCM2 promotes symmetric inheritance of modified histones during
1057 DNA replication. *Science* **361**, 1389-1391 (2018).
1058
1059 32. Kurat CF, Yeeles JTP, Patel H, Early A, Diffley JFX. Chromatin Controls DNA Replication
1060 Origin Selection, Lagging-Strand Synthesis, and Replication Fork Rates. *Mol Cell* **65**,
1061 117-130 (2017).
1062
1063 33. Kingston IJ, Yung JSY, Singleton MR. Biophysical Characterization of the Centromere-
1064 specific Nucleosome from Budding Yeast. *J Biol Chem* **286**, 4021-4026 (2011).
1065
1066 34. Lowary PT, Widom J. New DNA sequence rules for high affinity binding to histone
1067 octamer and sequence-directed nucleosome positioning. *J Mol Biol* **276**, 19-42 (1998).
1068
1069 35. van Loenhout MTJ, de Grunt MV, Dekker C. Dynamics of DNA Supercoils. *Science* **338**,
1070 94-97 (2012).
1071
1072 36. Ederth J, Artsimovitch I, Isaksson LA, Landick R. The downstream DNA jaw of bacterial
1073 RNA polymerase facilitates both transcriptional initiation and pausing. *J Biol Chem*
1074 **277**, 37456-37463 (2002).
1075
1076 37. Dyer PN*, et al.* Reconstitution of nucleosome core particles from recombinant histones
1077 and DNA. *Method Enzymol* **375**, 23-44 (2004).
1078
1079 38. Cotton RW, Hamkalo BA. Nucleosome Dissociation at Physiological Ionic Strengths.
1080 *Nucleic Acids Res* **9**, 445-457 (1981).
1081
1082 39. Ali FA*, et al.* Cryo-EM structure of a licensed DNA replication origin. *Nature*
1083 *Communications* **8**, (2017).
1084
1085 40. Frigola J, Remus D, Mehanna A, Diffley JFX. ATPase-dependent quality control of DNA
1086 replication origin licensing. *Nature* **495**, 339-343 (2013).
1087
1088 41. Candelli A*, et al.* Visualization and quantification of nascent RAD51 filament formation
1089 at single-monomer resolution. *P Natl Acad Sci USA* **111**, 15090-15095 (2014).
1090
1091 42. Forget AL, Dombrowski CC, Amitani I, Kowalczykowski SC. Exploring protein-DNA
1092 interactions in 3D using in situ construction, manipulation and visualization of
1093 individual DNA dumbbells with optical traps, microfluidics and fluorescence
1094 microscopy. *Nat Protoc* **8**, 525-538 (2013).
1095

43. Bustamante C, Marko JF, Siggia ED, Smith S. Entropic Elasticity of Lambda-Phage DNA. *Science* **265**, 1599-1600 (1994).

44. Jaqaman K*, et al.* Robust single-particle tracking in live-cell time-lapse sequences. *Nat Methods* **5**, 695-702 (2008).

45. Virtanen P*, et al.* SciPy 1.0: fundamental algorithms for scientific computing in Python (vol 33, pg 219, 2020). *Nat Methods* **17**, 352-352 (2020).

46. Truong C, Oudre L, Vayatis N. Selective review of offline change point detection methods. *Signal Process* **167**, (2020).

47. Michalet X. Mean square displacement analysis of single-particle trajectories with localization error: Brownian motion in an isotropic medium (vol 82, 041914, 2010). *Phys Rev E* **83**, (2011).

48. Odijk T. Stiff Chains and Filaments under Tension. *Macromolecules* **28**, 7016-7018 (1995).

49. Wallis S. Binomial Confidence Intervals and Contingency Tests: Mathematical Fundamentals and the Evaluation of Alternative Methods. *J Quant Linguist* **20**, 178-208 (2013).

50. Seabold S, Perktold J. Statsmodels: Econometric and Statistical Modeling with Python. *PROC OF THE 9th PYTHON IN SCIENCE CONF (SCIPY 2010)*, (2010).

ACKNOWLEDGMENTS

We thank Anne Early and Lucy Drury for providing yeast strains, Nerea Murugarren for assistance in loading bulk biochemical assays, Fiona Horne and Emilie van Vet for preliminary chromatin assembly experiments, and Alessandro Costa for useful discussions. ZL acknowledges the support given by EMBO Postdoctoral Fellowship (ALTF 484-2022). ND acknowledges funding from the Netherlands Organization for Scientific Research (NWO) through Top grant 714.017.002), 'BaSyC—Building a Synthetic Cell' Gravitation grant (024.003.019) of the Netherlands Ministry of Education, Culture and Science (OCW), and from the European Research Council through an Advanced Grant (REPLICHROMA; grant number 789267.

1138 **AUTHOR CONTRIBUTIONS**

1139 HS, JD, and ND conceived the study, and ND supervised the study. HS designed the
1140 experiments with input from ZL, EvV, JD, and ND. JD provided cell strains and advised on
1141 protein purification and biochemical conditions. TvL engineered DNA substrates, purified the
1142 proteins, and performed bulk biochemical assays. HS labeled the proteins and assembled
1143 chromatin substrates. HS performed all single-molecule experiments. ZL and EvV designed
1144 and wrote data analysis routines. HS and EvV also performed data analysis, with input from
1145 ZL and ND. All authors were involved in discussion of the data. HS and ND wrote the
1146 manuscript with input from the other authors.

1147

1148 **COMPETING INTERESTS**

1149 The authors declare no competing interests.

1150

1151 **FIGURES**

1152

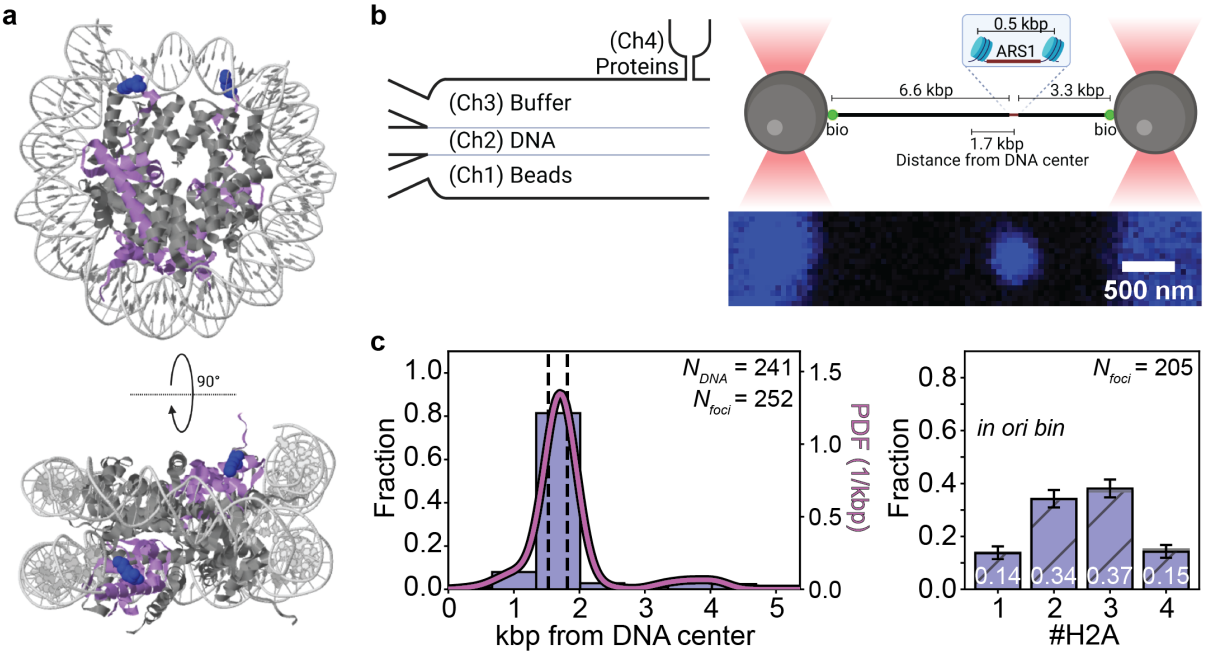

1153
1154

1155 **Figure 1. Design and characterization of a labeled chromatinized origin within 10.4 kbp DNA.**

1156 **(a)** Structural depictions of the yeast nucleosome (PDB: 1ID3), including in blue the mutated

1157 residues on the H2A histones for adding fluorescent labels. **(b)** (left panel) Schematic of the

1158 flow cell used in the single-molecule experiments. (right upper panel) Schematic of the 10.4

1159 kb DNA held in an optical trap that contains the ARS1 origin of replication flanked by two

1160 nucleosome positioning sites (NPSs). The DNA is chromatinized via salt gradient dialysis prior

1161 to its introduction into the single-molecule flow cell (**Supplementary Figure 1.2**). (right lower

1162 panel) Confocal scan showing that signal from fluorescently labeled H2A histones is detected

1163 as a single diffraction-limited spot localized at the NPSs. **(c)** (left panel) Spatial distribution of

1164 fluorescently labeled H2A on DNA described in panel (b), as deduced from the blue

1165 diffraction-limited spots (N_{foci}) collected from 248 distinct DNA molecules (N_{DNA}). Dashed lines

1166 indicate the location of the NPSs, and the solid curve indicates the kernel density estimation

1167 of the data. (right panel) Stoichiometry distribution of fluorescently labeled H2A histones in

1168 the bin containing the chromatinized origin. Error bars are one-sigma Wilson confidence
1169 intervals. White numbers inside the bars designate the fitted values based on the model
1170 described in the Methods and in **Supplementary Figure 1.3**. Data in both panels derives from
1171 four chromatinized samples (**Supplementary Figure 1.4**).
1172

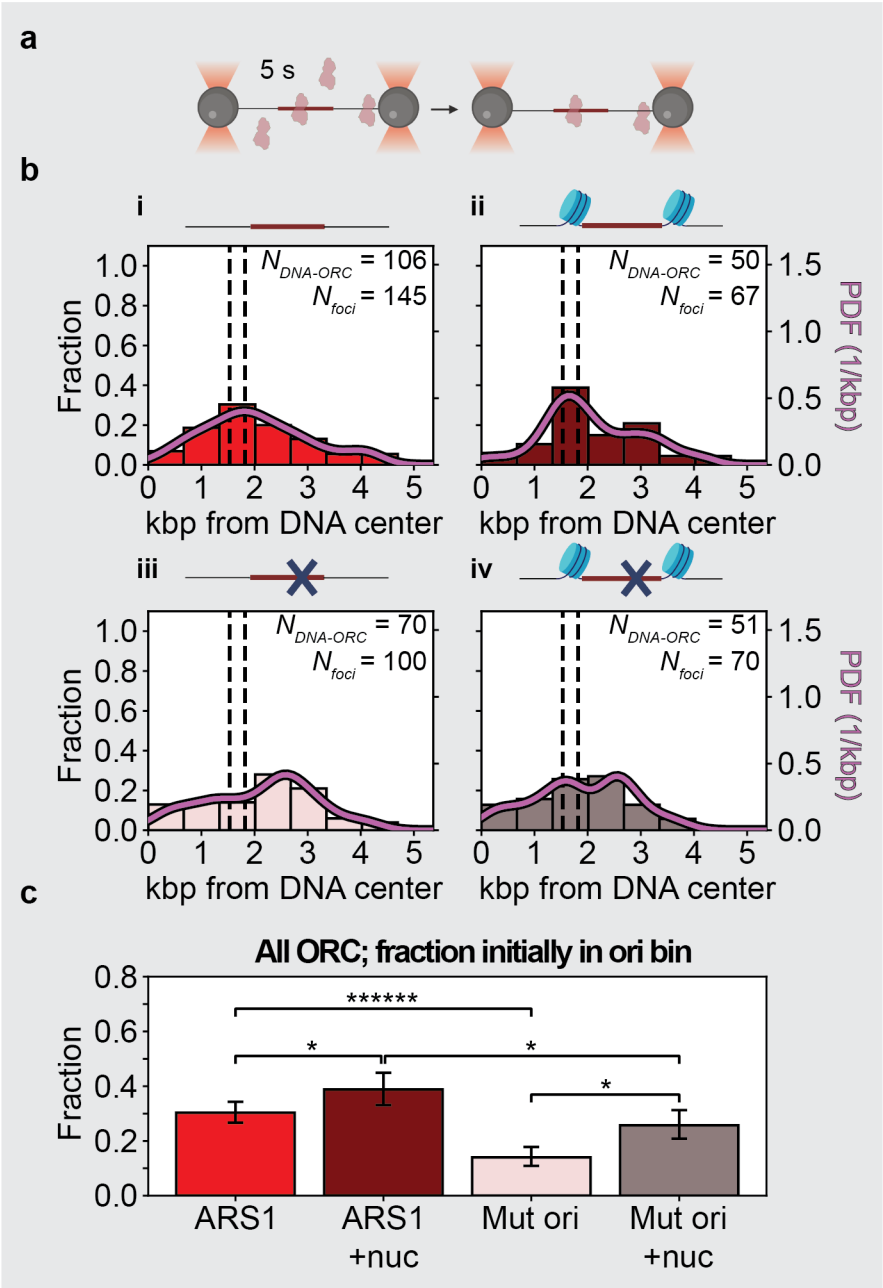

Figure 2. Spatial distribution of rapidly bound ORC on 10.4 kbp DNA containing a chromatinized origin. (a) Incubation method pertaining to data in panels (b-c). Tethered DNA molecules (chromatinized or not, as indicated) are introduced into protein channel (Ch4) for incubation with ORC and Cdc6 for 5 s in the presence of ATP, and then moved into the buffer channel (Ch3) for confocal scanning (see **Figure 1b** for schematic of the flow cell). **(b)** (i) Spatial distribution of ORC on DNA containing a non-chromatinized origin as deduced from the red

1181 diffraction-limited spots (N_{foci}) collected from 106 distinct DNA molecules ($N_{DNA\text{-}ORC}$). The
1182 dashed lines indicate the location of the NPSs, and the solid curve indicates the kernel density
1183 estimation of the data. (ii) Spatial distribution of ORC on DNA containing a chromatinized
1184 origin as deduced from the red diffraction-limited spots (N_{foci}) collected from 50 distinct DNA
1185 molecules ($N_{DNA\text{-}ORC}$) analyzed and displayed as in panel (b-i). (iii) Spatial distribution of ORC
1186 on DNA containing a non-chromatinized mutated origin as deduced from the diffraction-
1187 limited red spots (N_{foci}) collected from 70 distinct DNA molecules ($N_{DNA\text{-}ORC}$) analyzed and
1188 displayed as in panel (b-i). (iv) Spatial distribution of ORC on DNA containing a chromatinized
1189 mutated origin as deduced from the red diffraction-limited spots (N_{foci}) collected from 51
1190 distinct DNA molecules ($N_{DNA\text{-}ORC}$) analyzed and displayed as in panel b-i. **(c)** ORC occupancy
1191 probability for the bins containing the (chromatinized or not) origin in panels (b-i)-(b-iv). Error
1192 bars are one-sigma Wilson confidence intervals. Statistical significance is determined by a
1193 two-sided binomial test: * $p < 0.05$, ****** $p < 0.0000005$.
1194

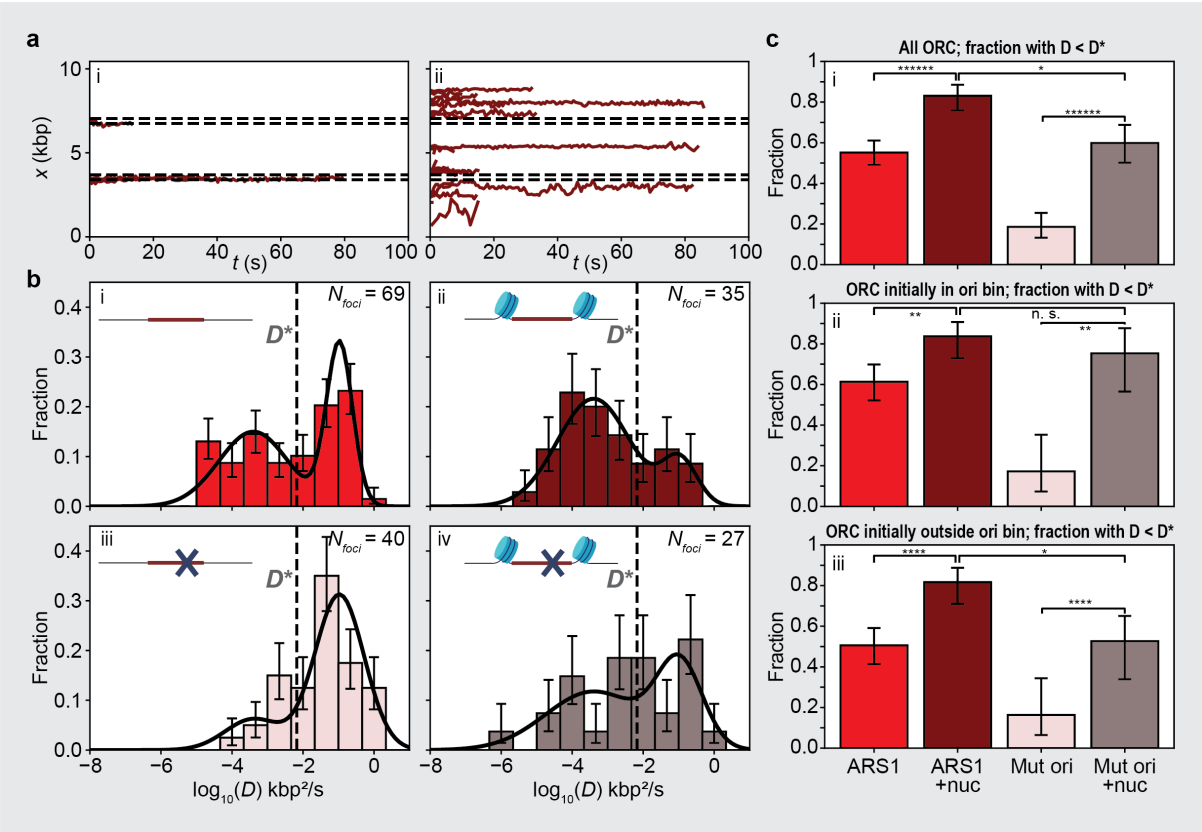

Figure 3. Mobility of ORC on 10.4 kbp DNA containing a chromatinized origin. (a) Traces collected on DNA containing a chromatinized origin illustrating motion of JF646-ORC (i) initially localized within the bin containing the chromatinized origin or (ii) initially localized elsewhere. **(b)** Histograms of the diffusion constants of ORC on DNA molecules containing (i) a non-chromatinized origin, (ii) a chromatinized origin, (iii) a non-chromatinized mutated origin, and (iv) a chromatinized mutated origin. Only foci containing 1 or 2 ORC are included in the analysis (N_{foci}). Error bars are one-sigma Wilson confidence intervals. The observed bimodal distribution is fitted to a double log-normal function (solid black line) which identifies a slowly moving or static ORC subpopulation (55% of the distribution with 0.0049 ± 0.0028 kbp^2/s, mean ± SEM) and a fast diffusive ORC subpopulation (0.152 ± 0.023 kbp^2/s, mean ± SEM). The dashed line indicates the average of the means of the two normal distributions used to fit $\log_{10}(D)$; this average is used as a threshold (D^*). The means of these

subpopulations are imposed in the fits to the data in panels (ii-iv). **(c)** Examination of the slowly moving or static ORC subpopulation. (i) Fitted proportion of the slowly moving or static ORC subpopulation for the datasets in panels (b-i)-(b-iv). (ii) The subpopulation of ORC initially localized within the bin containing the (chromatinized or not) origin was extracted from the dataset; the fraction of this subpopulation that is slowly moving or static ($D < D^*$) is shown here. (iii) The subpopulation of ORC initially localized outside the bin containing the (chromatinized or not) origin was extracted from the dataset; the fraction of this subpopulation that is slowly moving or static ($D < D^*$) is shown here. Error bars are one-sigma Wilson confidence intervals. Statistical significance is determined by a two-sided binomial test: n. s. not significant, * $p < 0.05$, ** $p < 0.005$, **** $p < 0.00005$, ***** $p < 0.000005$ ****** $p < 0.0000005$.

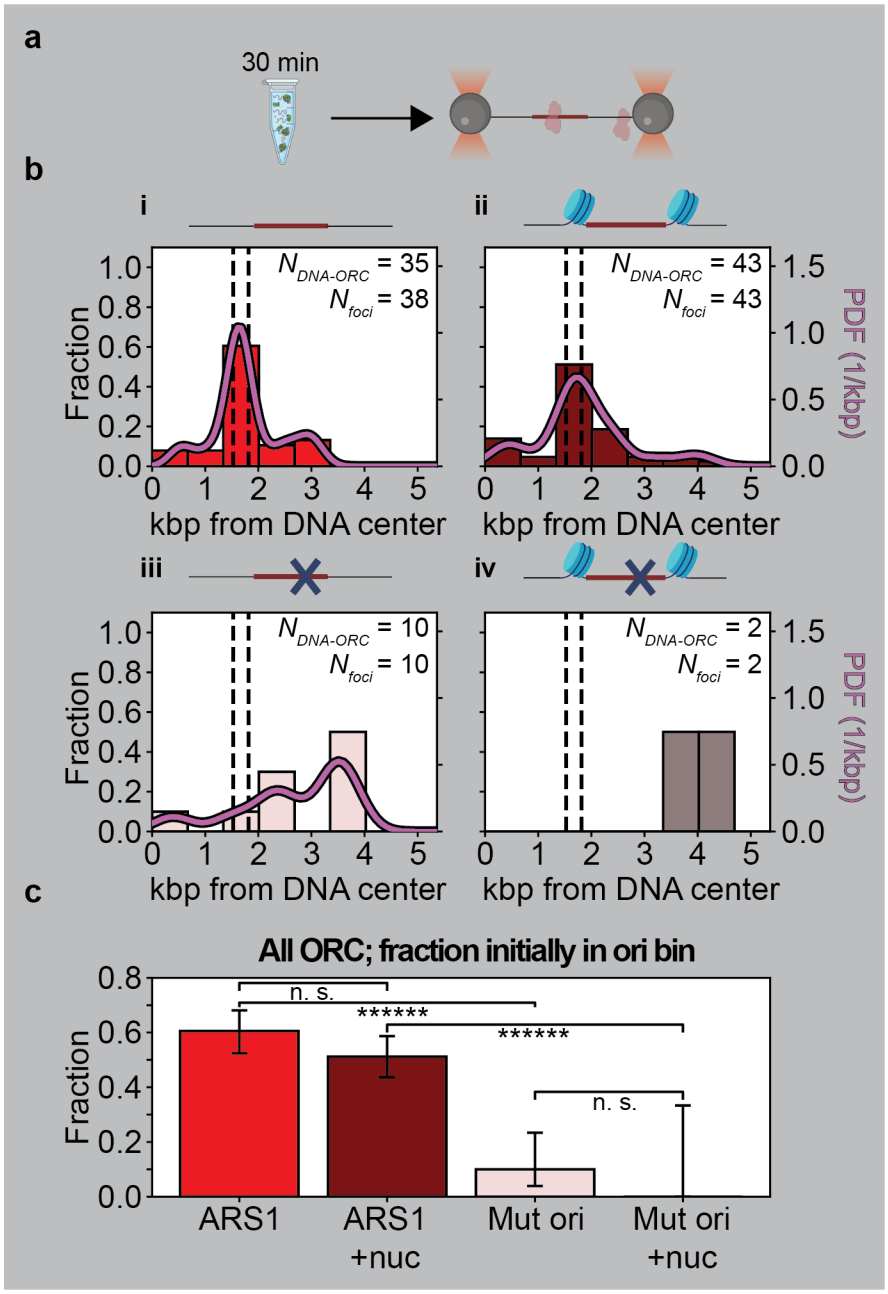

Figure 4. Spatial distribution of stably bound ORC on 10.4 kbp DNA containing a chromatinized origin. (a) Incubation method pertaining to data in panels (b-c). ORC and Cdc6 are incubated with DNA molecules (chromatinized or not, as indicated) in bulk for 30 min in the presence of ATP. Subsequently, the DNA-protein construct is flushed into the single-molecule flow cell, tethered, and moved into the buffer channel for confocal scanning. **(b)** (i) Spatial distribution of ORC on DNA containing a non-chromatinized origin as deduced from

1229 the diffraction-limited red spots (N_{foci}) collected from 35 distinct DNA molecules ($N_{DNA\text{-}ORC}$)
1230 analyzed and displayed as in panel (b-i). (ii) Spatial distribution of ORC on DNA containing a
1231 chromatinized origin as deduced from the diffraction-limited red spots (N_{foci}) collected from
1232 43 distinct DNA molecules ($N_{DNA\text{-}ORC}$) analyzed and displayed as in panel (b-i). (iii) Spatial
1233 distribution of ORC on DNA containing a non-chromatinized mutated origin as deduced from
1234 the diffraction-limited red spots (N_{foci}) collected from 10 distinct DNA molecules ($N_{DNA\text{-}ORC}$)
1235 analyzed and displayed as in panel (b-i). (iv) Spatial distribution of ORC on DNA containing a
1236 chromatinized mutated origin as deduced from the red diffraction-limited spots ($N_{DNA\text{-}ORC}$)
1237 collected from 2 distinct DNA molecules ($N_{DNA\text{-}ORC}$) analyzed and displayed as in panel (b-i).
1238 The dashed lines indicate the location of the NPSs, and the solid curve indicates the kernel
1239 density estimation of the data. **(c)** ORC occupancy probability for the bins containing the
1240 (chromatinized or not) origin in panels (b-i)-(b-iv). Error bars are one-sigma Wilson confidence
1241 intervals. Statistical significance is determined by a two-sided binomial test. n.s. not
1242 significant, ****** $p < 0.0000005$.
1243

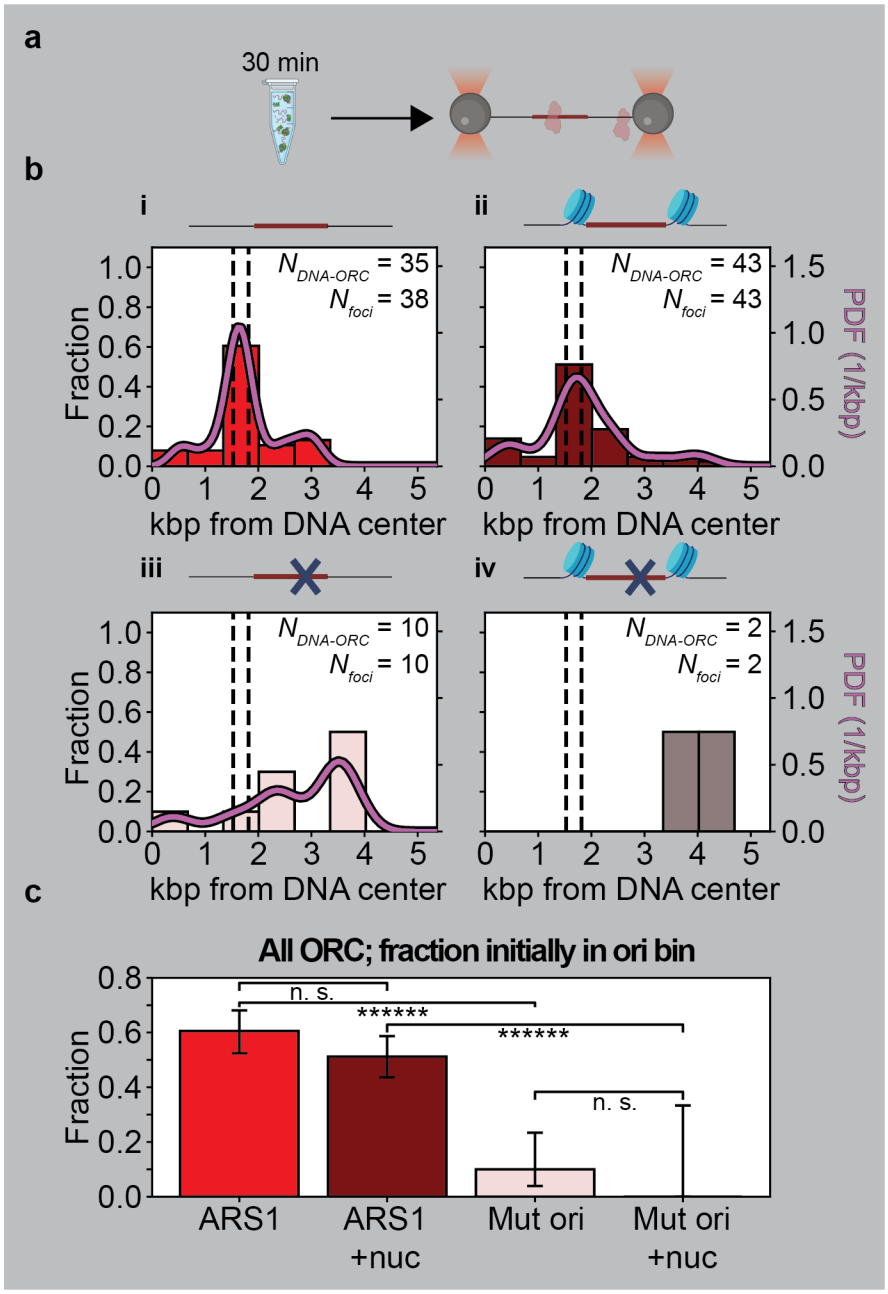

1244

1245

1246 **Figure 5. Nucleosomes spatially constrain MCM at the origin. (a)** ORC, Cdc6, and Mcm2-

1247 7/Cdt-1 are incubated with 10.4 kb DNA molecules (chromatinized or not, as indicated) in bulk

1248 for 30 min in the presence of ATP. Subsequently, the DNA-protein construct is flushed into

1249 the single-molecule flow cell, tethered and moved into the buffer channel for confocal

1250 scanning with an acquisition frequency of one frame every 0.01 min (t_f = 0.01 min). **(b)** (i)

1251 Spatial distribution of Mcm2-7 on DNA containing a non-chromatinized origin as deduced

1252 from the diffraction-limited red spots (N_{foci}) collected from 44 distinct DNA ($N_{DNA\text{-}MCM}$). The
1253 dashed lines indicate the location of the NPSs, and the solid curve indicates the kernel density
1254 estimation of the data. (ii) Spatial distribution of Mcm2-7 on DNA containing a chromatinized
1255 origin as deduced from the diffraction-limited red spots (N_{foci}) collected from 77 distinct DNA
1256 molecules ($N_{DNA\text{-}MCM}$) analysed and displayed as in panel (b-i). (iii) Spatial distribution of
1257 Mcm2-7 on DNA containing a non-chromatinized mutated origin as deduced from the
1258 diffraction-limited red spots (N_{foci}) collected from 65 distinct DNA molecules ($N_{DNA\text{-}MCM}$)
1259 analyzed and displayed as in panel (b-i). (iv) Spatial distribution of Mcm2-7 on DNA containing
1260 a chromatinized mutated origin as deduced from the diffraction-limited red spots (N_{foci})
1261 collected from 71 distinct DNA molecules ($N_{DNA\text{-}MCM}$) analyzed and displayed as in panel (b-i).
1262 **(c)** Mcm2-7 occupancy probability for the bins containing the (chromatinized or not) origin
1263 for the datasets in panels (b-i)-(b-iv). Error bars are one-sigma Wilson confidence intervals.
1264 Statistical significance is determined by a two-sided binomial test: n.s. not significant and
1265 ****** $p < 0.0000005$. **(d)** ORC, Cdc6, and Mcm2-7/Cdt-1 are incubated with 10.4 kb
1266 chromatinized DNA molecules in bulk for 30 min in the presence of ATP. Subsequently, the
1267 DNA-protein construct is flushed into the single-molecule flow cell, tethered and moved into
1268 the buffer channel for confocal scanning with an acquisition frequency of one frame per
1269 minute (t_f = 1 min). **(e)** Histograms of the relative displacements (Δx = 2 min) between 2 min
1270 intervals (Δt = 2 min) for (i) dCas9 molecules over the entire lifetime of the fluorophore for
1271 dCas9 molecules, (ii) for Mcm2-7 on DNA containing a non-chromatinized origin or (iii)
1272 chromatinized origin. For all three panels, acquisition is continued until the fluorophore is
1273 bleached (~20 min). N_{foci}, number of molecules; $N_{\Delta x}$, number of relative displacements; σ,
1274 standard deviation.